🎓 GRADA: GRADIENT-GUIDED KNOWLEDGE DISTILLATION FOR DOMAIN ADAPTATION

Anonymous authors
Paper under double-blind review

ABSTRACT

In this paper, we explore **how to enhance student network performance in knowledge distillation (KD) for domain adaptation (DA)**. We identify two key factors impacting student performance under domain shift: **(1) the capability of the teacher network** and **(2) the effectiveness of the knowledge distillation strategy**. For the first factor, we integrate a Vision Transformer (ViT) as the feature extractor and our proposed Category-level Aggregation (CA) module as the classifier to construct the ViT+CA teacher network. This architecture leverages ViT's ability to capture detailed representations of individual images. Additionally, the CA module employs the message-passing mechanism of a graph convolutional network to promote intra-class relations and mitigate domain shift by grouping samples with similar class information. For the second factor, we leverage pseudo labels generated by the ViT+CA teacher to guide the gradient updates of the student network's parameters, aligning the student's behavior with that of the teacher. To optimize for efficient inference and reduced computational cost, we use a convolutional neural network (CNN) for feature extraction and a multilayer perceptron (MLP) as the classifier to build the CNN+MLP student network. Extensive experiments on various DA datasets demonstrate that our method significantly surpasses state-of-the-art approaches. Our code will be available soon.

1 INTRODUCTION

Domain adaptation (DA) has attracted significant attention in recent research due to its potential to mitigate domain shift (Ben-David et al., 2010) between source and target domains, enabling the transfer of knowledge from labeled source data to unlabeled target data. Traditional DA methods primarily rely on convolutional neural networks (CNNs) (Kayhan & van Gemert, 2020) to learn domain-invariant representations. However, studies (Li et al., 2017; Naseer et al., 2021) indicate that CNN-based models are highly sensitive to domain shift. Recently, DA approaches based on Vision Transformers (ViTs) (Yang et al., 2023; Xu et al., 2022) have demonstrated superior performance over CNN-based methods (Xiao et al., 2023; Yu & Lin, 2023). While these approaches mark significant progress, deploying ViT-based models in real-world applications remains challenging, especially in scenarios demanding rapid inference, minimal storage, and lower computational costs, such as on resource-constrained devices. In contrast, compact CNN models like ResNet18 and ResNet34 (He et al., 2016) are often preferred for their efficiency. This raises an intuitive question: '*how can we collaboratively leverage the strengths of these two models within a unified framework?*' Specifically, '*can we utilize the strong representational capability of the ViT-based model during training while exploiting the computational efficiency of the CNN-based model during inference?*' This balance would meet the demands for high performance with low computational cost. Knowledge distillation (KD) offers a promising strategy to address this concern described as: **Teacher (ViT)** $\xrightarrow{\textit{Method}}$ **Student (CNN)**. Herein, the knowledge acquired by the ViT-based teacher model is transferred to a compact CNN-based student model. We identify two critical factors that directly impact the performance of the student model: ① **the ability of the ViT-based teacher** and ② **the effectiveness of the teaching method**.

To satisfy ①, the teacher must perform effectively on labeled source data, demonstrating low training loss and robustness to domain shift. Following prior DA methods (Xu et al., 2022; Yang et al., 2023), we employ a ViT model as the feature extractor, leveraging its strong representational capacity. However, these methods typically use a multilayer perceptron (MLP) as the classification head, which may have limited generalization due to its inability to capture relational information among neighboring samples. To address this limitation, we propose a Category-level Aggregation (CA) module, inspired by graph convolutional networks (GCNs) (Kipf & Welling, 2017), as the classification head to form the ViT+CA teacher network. The CA module enhances the teacher network's generalization by effectively capturing *intra-class relations*. Specifically, it enriches source features extracted by the ViT-based model through a message-passing mechanism guided by ground-truth labels. Similarly, the CA module improves intra-class information in the target domain based on pseudo labels generated from unlabeled target data. Additionally, it constructs a cross-domain knowledge graph, aligning unlabeled target samples with labeled source samples by *class-aware feature alignment*, where pseudo labels and source ground-truth labels share the same categories. By doing so, the teacher network not only captures structural representations within both domains but also reduces the discrepancy between them.

Regarding ②, employing ViT and CNN in a teacher-student paradigm, it introduces a cross-architecture challenge due to their distinct mechanisms. CNN-based models capture local image features through convolutional operations (Kayhan & van Gemert, 2020), whereas ViT-based models, via self-attention mechanisms, effectively learn global information (Dosovitskiy et al., 2021). Therefore, applying a feature-based KD approach (Heo et al., 2019; Chen et al., 2021) with the ViT-CNN pair requires additional transformation steps. While logit distillation (Hinton, 2015; Huang et al., 2022) may serve as an alternative, traditional logit-based KD approaches typically align the teacher and student networks by focusing on specific model weights corresponding to regions within the logit space. Consequently, the performance of the knowledge distillation process remains suboptimal. To address this problem, we propose a KD method named **Gra**dient-Guided Knowledge Distillation for **D**omain **A**daptation (**GraDA**). Drawing inspiration from (Wang et al., 2022), this approach emphasizes gradient knowledge distillation, where all weights of the student network are considered, and the teacher network guides the gradient direction to update the student's weights effectively. Specifically, in GraDA, the teacher network guides the student solely through pseudo labels, giving the student network flexibility to learn class representations on its own. This insight aligns with successful teaching strategies in education (Tan & Abbas, 2009), where teachers leave space for students to discover and solve problems on their own under guidance, rather than encouraging mechanical imitation. Moreover, teachers are expected to continuously expand their knowledge and teaching skills to provide higher-quality instruction. Notably, the student network in our method remains consistent with prior DA approaches (Jin et al., 2020; Li et al., 2021a), utilizing a CNN-based feature extractor and an MLP as the classifier (CNN+MLP). As illustrated in Fig. 1, our method is effective, particularly when the teacher and student networks yield similar classification results, surpassing existing logit-based methods.

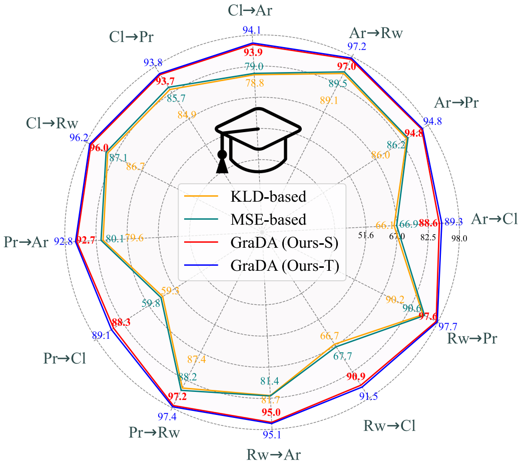

Figure 1: Comparison results of various knowledge distillation methods with our GraDA on **Office-Home** (Venkateswara et al., 2017) under UDA.

In summary, our key contributions are three-fold:

- We design a strong teacher network that provides robust representations by enriching intra-class relations within each domain and mitigating domain shift across domains through class-aware feature alignment.

- We introduce gradient-guided knowledge distillation, allowing the student network to behave similarly to its teacher following its own capacity constraints, thus reducing cross-architecture and capability gaps.

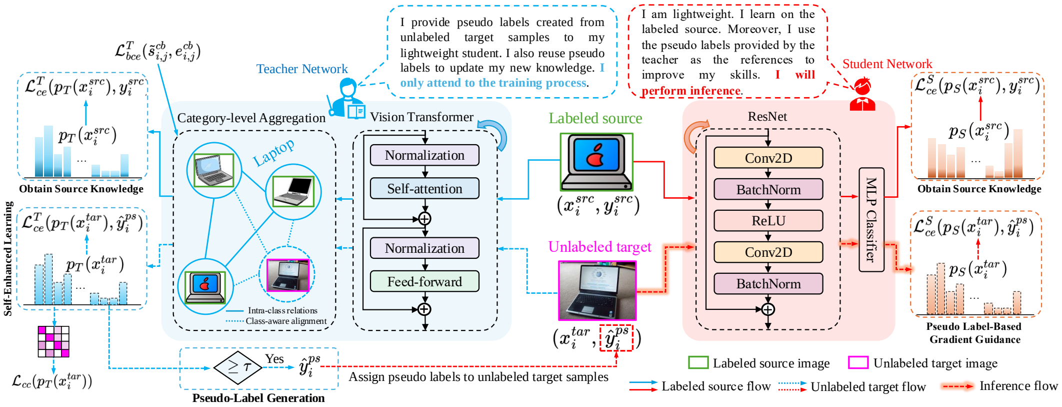

I provide pseudo labels created from unlabeled target samples to my lightweight student. I also reuse pseudo labels to update my new knowledge. **I only attend to the training process**.

I am lightweight. I learn on the labeled source. Moreover, I use the pseudo labels provided by the teacher as the references to improve my skills. **I will perform inference**.

Figure 2: Illustration of the proposed GraDA. The teacher network includes a ViT-based model with a CA module, while the student network comprises a CNN-based model and an MLP. The teacher uses pseudo labels to guide the gradient direction for updating the student's parameters. Notably, the teacher is involved only during training, whereas the student is used for testing.

- Our proposed method is evaluated through quantitative and qualitative analyses, achieving state-of-the-art results across various DA tasks on popular datasets: **VisDA2017**, **Office-Home**, and **DomainNet**.

2 Related Works

CNN/ViT-based in Domain Adaptation. Traditional DA methods (Ganin et al., 2016; Saito et al., 2018) utilize convolutional neural networks (CNN) to learn domain-invariant and discriminative features. However, studies (Li et al., 2017; Naseer et al., 2021) have revealed that convolutional layers are sensitive to domain shift. More recently, ViT-based DA methods (Xu et al., 2022; Zhu et al., 2023a) have demonstrated that vision transformers (ViT) can effectively reduce the discrepancy between source and target domains, leading to significant improvements in performance. For instance, CDTrans (Xu et al., 2022) illustrates that the cross-attention mechanism within ViT can counteract domain shift. Consequently, ViT-based DA approaches can generate accurate pseudo labels that help mitigate domain shift via class-aware feature alignment. However, their memory-intensive attention mechanism makes them computationally costly and hard to deploy in real-world settings.

Knowledge Distillation. Over the past decade, KD methods have been mainly categorized into two types: logit-based (Hinton, 2015; Zhao et al., 2022; Huang et al., 2022) and feature-based (Heo et al., 2019; Romero et al., 2015; Chen et al., 2021). While logit-based approaches focus on narrowing the logit distribution between teacher and student networks, feature-based methods encourage the student to mimic the teacher's representations. However, these techniques, particularly feature-based approaches, struggle to transfer knowledge between networks with differing properties (Liu et al., 2022b), like ViT and CNN, due to low feature space similarity. (Zhu et al., 2023b) attempted to address this by using both feature- and logit-based mechanisms for cross-architecture knowledge distillation, though additional transformation steps are required. Nonetheless, both logit-based and feature-based methods operate in the same point-wise manner, where only specific parts of the student's weights are considered to match the teacher.

3 Methodology

3.1 Problem Formulation

In unsupervised domain adaptation (UDA), we are given the source dataset $D_{src} = \{(x_i^{src}, y_i^{src})\}_{i=1}^{N_{src}}$, with N_{src} representing the number of source samples. Each source image x_i^{src} corresponds to an individual data point paired with a label $y_i^{src} \in [C]$. Here, $C \in \mathbb{Z}^+$ indicates the number of categories, and $[C]$ denotes the set $\{1, 2, \ldots, C\}$. Additionally, we are also provided with unlabeled target data, denoted as $D_{tar} = \{(x_i^{tar})\}_{i=1}^{N_{tar}}$, where x_i^{tar} represents a target image, and N_{tar} denotes the number of target samples. The model is trained on both D_{src} and D_{tar}, to achieve strong performance on D_{tar}. It is important to emphasize that D_{src} and D_{tar} share the same categories, and the target label $y_i^{tar} \in [C]$ is only used during the testing phase. The architecture and training process are illustrated in Fig. 2.

3.2 Teacher Network

Architecture. *To match* ①, we use ViT (Dosovitskiy et al., 2021) as the backbone (f_{vit}) for its superior global pattern capture via self-attention compared to CNNs (Kayhan & van Gemert, 2020). For the classification head, we introduce a Category-level Aggregation (CA) module, drawing inspiration from GCNs (Kipf & Welling, 2017), to enhance representations through message passing. The CA module comprises f_{sim}, which computes similarity scores, and f_{agg}, which aggregates feature vectors within a mini-batch.

Operation. During training, the input data is divided into multiple mini-batches of size B. Each training sample $x_i \in \mathbb{R}^{H\times W\times 3}$ is first encoded by f_{vit}: $z_i^{vit} = f_{vit}(x_i; \theta_{vit}) \in \mathbb{R}^d$, where z_i^{vit} is a feature vector, d is the embedding size, and θ_{vit} is the set of learnable parameters of f_{vit}. The batch of feature vectors $\{(z_i^{vit})\}_{i=1}^{B}$ is then processed by f_{sim} and f_{agg} in the CA module for feature aggregation. Specifically, $f_{sim} : \mathbb{R}^d \to \mathbb{R}^1$ is used to identify neighboring instances within the mini-batch by calculating similarity scores as:

$$\hat{s}_{i,j} = \texttt{sigmoid}\big(f_{sim}(\|z_i^{vit} - z_j^{vit}\|; \theta_{sim})\big), \tag{1}$$

where $\hat{s}_{i,j}$ is a scalar value that quantifies the level of relationship between the i-th and j-th feature vectors. θ_{sim} is the set of learned parameters of f_{sim}. The correlations among samples within a mini-batch are stored in the similarity matrix $\hat{S} \in \mathbb{R}^{B\times B}$, where $\hat{s}_{i,j} \in \hat{S}$. We normalize $\hat{S}$ by adding the self-connections formulated as follows:

$$\tilde{S} = D^{-\frac{1}{2}}(\hat{S} + I)D^{-\frac{1}{2}}, \tag{2}$$

where I denotes the identity matrix, and D represents the degree matrix of $\hat{S}+I$. Finally, the feature aggregation is processed as follows:

$$z_i^T = f_{agg}\Big(\big[z_i^{vit}, \sum_{j\in B} \tilde{s}_{i,j} \cdot z_j^{vit}\big]; \theta_{agg}\Big), \tag{3}$$

where z_i^T is an aggregated feature vector of the teacher network with the C-dimensional logit for the final prediction. $[\cdot]$ denotes the concatenation operation and $\tilde{s}_{i,j} \in \tilde{S}$. $f_{agg} : \mathbb{R}^{2d} \to \mathbb{R}^C$ is the linear projection and θ_{agg} is the set of learnable parameters of f_{agg}.

3.3 Student Network

Architecture. We attempt to build a straightforward network that meets the requirement for fast inference. Thus, we select the CNN-based model as the feature extractor, f_{cnn}, followed by an MLP as the classification head.

Operation. f_{cnn} takes each mini-batch $\{(x_i)\}_{i=1}^{B}$ as input, and x_i is encoded as $z_i^{cnn} = f_{cnn}(x_i; \theta_{cnn}) \in \mathbb{R}^{d'}$, where z_i^{cnn} denotes the feature vector extracted by f_{cnn} with the dimensional embedding of size d', which is parameterized by θ_{cnn}. Next, the MLP classifier processes z_i^{cnn} to produce the predicted vector $p_S(x_i) = \texttt{softmax}(\text{MLP}(z_i^{cnn}; \theta_{mlp}))$, where θ_{mlp} is the set of learned parameters of MLP.

3.4 Training Strategy for Teacher Network

We conduct a three-step approach in the teacher network: *1) Enriching Intra-Class Relations*, *2) Pseudo-Label Generation*, and *3) Self-Enhanced Learning*, intending to improve feature representations and mitigate the domain shift issue.

Enriching Intra-Class Relation. The teacher network exploits the relationships among labeled samples within each mini-batch $\{(x_i, y_i)\}_{i=1}^{B}$, thereby enhancing intra-class information. To be specific, we train f_{sim} to explore the pairwise similarity between the samples within the mini-batch using a binary cross-entropy (*bce*) loss as follows:

$$\mathcal{L}_{bce}^{T}(\tilde{s}_{i,j}, e_{i,j}) = -e_{i,j}\log(\tilde{s}_{i,j}) - (1-e_{i,j})\log(1-\tilde{s}_{i,j}), \tag{4}$$

where $e_{i,j}$ represents the ground-truth of edge, $e_{i,j} = 1$ indicates that the samples x_i and x_j belong to the same category ($y_i = y_j$); otherwise, $e_{i,j} = 0$. $\tilde{s}_{i,j}$ is the similarity score between x_i and x_j predicted by f_{sim}. Next, we update the parameters of f_{agg} for feature aggregation using the cross-entropy (*ce*) as follows:

$$\mathcal{L}_{ce}^{T}(p_T(x_i), y_i) = -y_i \log\big(p_T(x_i)\big), \tag{5}$$

where $\mathcal{L}_{ce}^{T}$ denotes the cross-entropy loss function. $p_T(x_i) = \texttt{softmax}(z_i^T)$ indicates the prediction of x_i with the aggregated features z_i^T in Eq. (3), and $y_i \in [0,1]^C$ is the ground truth in one-hot encoding form.

We can easily adapt Eq. (4) and Eq. (5) on the labeled source $D_{src} = \{x_i^{src}, y_i^{src}\}_{i=1}^{N_{src}}$ to enrich intra-class relation of the source domain as follows.

$$\min_{\theta_{vit},\theta_{sim},\theta_{agg}} \mathcal{L}_{bce}^{T}(\tilde{s}_{i,j}^{src}, e_{i,j}^{src}) + \mathcal{L}_{ce}^{T}(p_T(x_i^{src}), y_i^{src}), \tag{6}$$

where $\mathcal{L}_{bce}^{T}(\tilde{s}_{i,j}^{src}, e_{i,j}^{src})$ and $\mathcal{L}_{ce}^{T}(p_T(x_i^{src}), y_i^{src})$ are the *bce* and *ce* losses used to update θ_{vit}, θ_{sim}, and θ_{agg} on the labeled source data, respectively. The proposed teacher network goes beyond obtaining the semantic features of individual images. Furthermore, it can comprehend the similarities between the neighboring samples, thus *enhancing intra-class consistency*. To enable intra-class relationships in the unlabeled target data, we assign pseudo-labels through a label generation process.

Pseudo-Label Generation. Following (Sohn et al., 2020), we first input the target image x_i^{tar} into the teacher network, and the resulting prediction $p_T(x_i^{tar})$ is then converted into a one-hot hard label as follows:

$$\hat{y}_i^{ps} = \texttt{argmax}\big(p_T(x_i^{tar})\big) \text{ if } \texttt{max}\big(p_T(x_i^{tar})\big) \geq \tau, \tag{7}$$

where τ is a confidence threshold that controls the quality of the generated pseudo labels. Thanks to Eq. (7), we can obtain a pseudo-labeled set: $D_{ps} = \{(x_i^{tar}, \hat{y}_i^{ps})\}_{i=1}^{N_{ps}}$ from the unlabeled set $D_{tar} = \{(x_i^{tar})\}_{i=1}^{N_{tar}}$, where N_{ps} denotes the number of pseudo labels and $N_{ps} \leq N_{tar}$.

Self-Enhanced Teacher Learning. In the next step, we combine $D_{ps} = \{(x_i^{tar}, \hat{y}_i^{ps})\}_{i=1}^{N_{ps}}$ into the source $D_{src} = \{(x_i^{src}, y_i^{src})\}_{i=1}^{N_{src}}$ as follows:

$$D_{cb} = D_{src} \cup D_{ps}, N_{cb} = N_{ps} + N_{src}, \tag{8}$$

where N_{cb} is the number of combined samples. Since the combined dataset D_{cb} consists of labeled data, it enables the use of supervised losses as described in Eq. (4) and Eq. (5). Therefore, Eq. (6) can be rewritten as follows:

$$\min_{\theta_{vit},\theta_{sim},\theta_{agg}} \mathcal{L}_{bce}^{T}(\tilde{s}_{i,j}^{cb}, e_{i,j}^{cb}) + \mathcal{L}_{ce}^{T}(p_T(x_i^{cb}), y_i^{cb}), \tag{9}$$

where $\tilde{s}_{i,j}^{cb}$ and $e_{i,j}^{cb}$ denote the similarity score and ground-truth edge of $\{(x_i^{cb}, y_i^{cb})\}_{i=1}^{N_{cb}} \in D_{cb}$, determined similarly to Equation Eq. (4). Notably, the teacher model enriches semantic representations and alleviates domain discrepancy when trained on D_{cb}, as it preserves intra-class relations in the source domain where $y_i^{src} = y_j^{src}$ within D_{cb}. Besides, it also leverages pseudo labels to exploit the intra-class relation of the target domain when $\hat{y}_i^{ps} = \hat{y}_j^{ps}$. Moreover, our teacher network addresses domain shift by *class-aware feature alignment* when D_{cb} includes pairs with $\hat{y}_i^{ps} = y_j^{src}$.

Furthermore, we minimize cross-class confusion (MCC) (Jin et al., 2020) on D_{tar} to enhance the pseudo-label generation process of the teacher network as follows:

$$\mathcal{L}_{cc}(p_T(x_i^{tar})) = \frac{1}{C}\sum_{c=1}^{C}\sum_{c'\neq c}^{C} |(p_T(x_{i,c}^{tar})^{\top}(p_T(x_{i,c'}^{tar})|, \tag{10}$$

where $p_T(x_{i,c}^{tar})$ and $p_T(x_{i,c'}^{tar})$ represent the probabilities of the target sample x_i^{tar} belonging to the c-th and c'-th classes, respectively, where $\{c, c'\} \in C$. $\mathcal{L}_{cc}(p_T(x_i^{tar}))$ is minimized to alleviate the cross-class confusion level between the c-th and c'-th classes of the target samples x_i^{tar}.

3.5 Training Strategy for Student Network

We also train the student network with the combined dataset $D_{cb} = \{(x_i^{cb}, y_i^{cb})\}_{i=1}^{N_{cb}}$ using the cross-entropy loss as:

$$\mathcal{L}_{ce}^{S}(p_S(x_i^{cb}), y_i^{cb}) = -y_i^{cb} \log\big(p_S(x_i^{cb})\big). \tag{11}$$

As defined in Eq. (8), D_{cb} consists of both D_{src} and D_{ps}. Thus, the student network can *Obtain Source Knowledge* on labeled source samples and effectively learn on unlabeled target data via *Pseudo Label-Based Gradient Guidance*.

Obtain Source Knowledge. The student network captures the knowledge in $D_{src} = \{(x_i^{src}, y_i^{src})\}_{i=1}^{N_{src}} \in D_{cb}$ using the cross-entropy loss as follows:

$$\mathcal{L}_{ce}^{S}(p_S(x_i^{src}), y_i^{src}) = -y_i^{src} \log(p_S(x_i^{src})), \tag{12}$$

where $p_S(x_i^{src}) = \texttt{softmax}\big(\text{MLP}(f_{cnn}(x_i^{src}))\big)$ represents the output prediction of the source image x_i^{src}, which can be rewritten as follows:

$$\min_{\theta_{cnn}, \theta_{mlp}} \mathcal{L}_{ce}^{S}(p_S(x_i^{src}), y_i^{src}). \tag{13}$$

The student's parameters θ_S including θ_{cnn} and θ_{mlp}.

Pseudo Label-Based Gradient Guidance. We use $D_{ps} = \{(x_i^{tar}, \hat{y}_i^{ps})\}_{i=1}^{N_{ps}} \in D_{cb}$ to adjust the gradient direction in updating the parameters of the student network as follows:

$$\theta_S \leftarrow \theta_S - \eta \nabla_{\theta_S} \mathcal{L}_{ce}^{S}(p_S(x_i^{tar}), \hat{y}_i^{ps}), \tag{14}$$

where ∇_{θ_S} is the gradient of the loss $\mathcal{L}_{ce}^{S}$ with respect to θ_S on the unlabeled target data with the learning rate η. The student network provides prediction on the target image x_i^{tar} by $p_S(x_i^{tar}) = \texttt{softmax}\big(\text{MLP}(f_{cnn}(x_i^{tar}))\big)$. $\hat{y}_i^{ps}$ refers to the pseudo label generated by teacher network using Eq. (7), which guides the gradient $\nabla_{\theta_S} \mathcal{L}_{ce}^{S}(p_S(x_i^{tar}), \hat{y}_i^{ps})$, distilling the knowledge from the teacher network to the student network. The goal of the gradient guidance strategy is to align the student's gradient directions with those of the teacher, ensuring the student behaves similarly. Consequently, the student converges toward the optimal solution alongside its teacher on the target data, satisfying *the factor* ②, as verified by the qualitative visualization in the analysis section.

3.6 Implementation Details

The training procedure of GraDA is processed in each episode e consisting of a fixed number of training steps t. Specifically, in the initial episode $(e = 0)$, D_{src} is sampled into multiple mini-batches of size B to facilitate training of both teacher and student networks as in Eq. (6) and Eq. (12), respectively. After completing the initial episode, the teacher network is utilized to generate the first pseudo-labeled set D_{ps}^1 from the unlabeled target data D_{tar} for the next episode $(e = 1)$ using Eq. (7). D_{ps}^1 is then combined with D_{src} to form $D_{cb}^1 = D_{src} \cup D_{ps}^1$, as specified in Eq. (8), which is summarized as follows:

$$D_{cb}^{e} = D_{src} \cup D_{ps}^{e}, \text{ where } D_{cb}^{0} = D_{src}. \tag{15}$$

Finally, D_{cb}^{e} is divided into mini-batches of size B to update the parameters of the teacher and student networks by using Eq. (9) and Eq. (11), respectively. This iterative process continues until convergence, where both networks align at an optimal point within a flattened region of the loss surface.

4 Experiments

4.1 Setup

Dataset. We conduct experiments on **VisDA2017** (Peng et al., 2018) with the domain adaptation task: *Synthetic* to *Real-world*. **Office-Home** (Venkateswara et al., 2017) includes 4 different domains: *Art* (Ar), *Clipart* (Cl), *Product* (Pr), and *Real-World* (Rw), providing 12 DA tasks. A subset

Net	Method	Mean
ResNet101	MCC (ECCV'20)	78.8
	STAR (CVPR'20)	82.7
	FixBi (CVPR'21)	87.2
	DAMP (CVPR'24)	88.4
	HVCLIP (ECCV'24)	90.0
	🎓 GraDA (S)	**96.5**
ViT-B	PMTrans (CVPR'23)	87.5
	SSRT (CVPR'22)	88.8
	DAMP (CVPR'24)	90.9
	NVC (WACV'24)	91.4
	HVCLIP (ECCV'24)	92.5
	🎓 GraDA (T)	**97.0**

(a) **VisDA2017**

Net	Method	Ar→Cl	Ar→Pr	Ar→Rw	Cl→Ar	Cl→Pr	Cl→Rw	Pr→Ar	Pr→Cl	Pr→Rw	Rw→Ar	Rw→Cl	Rw→Pr	Mean
ResNet50	SCDA (ICCV'21)	57.5	76.9	80.3	65.7	74.9	74.5	65.5	53.6	79.8	74.5	59.6	83.7	70.5
	DALN (CVPR'22)	57.8	79.9	82.0	66.3	76.2	77.2	66.7	55.5	81.3	73.5	60.4	85.3	71.8
	AML (IEEE Trans'23)	58.9	77.2	81.7	69.6	77.9	78.6	66.6	57.9	82.3	74.7	62.5	84.5	72.7
	GeT (ICCV'23)	59.4	79.6	82.9	71.4	79.8	79.8	69.7	56.2	83.5	73.9	60.1	86.0	73.5
	DAMP (CVPR'24)	59.7	88.5	86.8	76.6	88.9	87.0	76.3	59.6	87.1	77.0	61.0	89.9	78.2
	HVCLIP (ECCV'24)	62.0	85.8	86.2	77.8	84.3	86.8	80.7	66.5	87.8	80.3	64.9	90.4	79.5
	🎓 GraDA (S)	**88.6**	**94.8**	**97.0**	**93.9**	**93.7**	**96.0**	**92.7**	**88.3**	**97.2**	**95.0**	**90.9**	**97.6**	**93.8**
ViT-B	TVT (WACV'23)	74.9	86.8	89.5	82.8	88.0	88.3	79.8	71.9	90.1	85.5	74.6	90.6	83.6
	SSRT (CVPR'22)	75.2	89.0	91.1	85.1	88.3	90.0	85.0	74.2	91.3	85.7	78.6	91.8	85.4
	NVC (WACV'24)	75.1	89.0	91.5	86.4	88.6	90.2	84.8	73.7	91.7	87.1	74.6	92.9	85.5
	DAMP (CVPR'24)	75.7	94.2	92.0	86.3	94.2	91.9	86.2	76.3	92.4	86.1	75.6	94.0	87.1
	PMTrans (CVPR'23)	81.2	91.6	92.4	88.9	91.6	93.0	88.5	80.0	93.4	89.5	82.4	94.5	88.9
	HVCLIP (ECCV'24)	86.3	**96.4**	94.0	91.6	**97.9**	94.6	87.5	85.3	94.8	89.9	88.1	97.0	92.0
	🎓 GraDA (T)	**89.3**	94.8	**97.2**	**94.1**	93.8	**96.2**	**92.8**	**89.1**	**97.4**	**95.1**	**91.5**	**97.7**	**94.0**

(b) **Office-Home**

Table 1: Accuracy (%) on (a) **VisDA2017** and (b) **Office-Home** under the UDA setting. We compare the results of the student GraDA (S) to previous CNN-based works for fairness, while the comparison of the teacher GraDA (T) and ViT-based DA works is provided for reference. The best results are marked as **bold**. For **VisDA2017**, the per-class accuracy is in the *Suppl. Material*.

Net	Method	rel→clp		rel→pnt		pnt→clp		clp→skt		skt→pnt		rel→skt		pnt→rel		Mean	
		1-shot	3-shot	1-shot	3-shot	1-shot	3-shot	1-shot	3-shot	1-shot	3-shot	1-shot	3-shot	1-shot	3-shot	1-shot	3-shot
ResNet34	MME (ICCV'19)	70.0	72.2	67.7	69.7	69.0	71.7	56.3	61.8	64.8	66.8	61.0	61.9	76.1	78.5	66.4	68.9
	APE (ECCV'20)	70.4	76.6	70.8	72.1	72.9	76.7	56.7	63.1	64.5	66.1	63.0	67.8	76.6	79.4	67.6	71.7
	SPA (NIPS'23)	75.3	76.0	71.8	72.2	74.8	76.5	65.9	67.0	69.8	71.1	65.8	67.2	81.1	82.3	72.1	73.2
	GeT (ICCV'23)	76.1	77.6	72.5	73.9	73.9	75.8	66.7	67.8	69.8	73.6	66.8	67.1	82.0	82.8	72.2	73.9
	DECOTA (ICCV'21)	79.1	80.4	74.9	75.2	76.9	78.7	65.1	68.6	72.0	72.7	69.7	71.9	79.6	81.5	73.9	75.6
	CDAC (CVPR'21)	77.4	79.6	74.2	75.1	75.5	79.3	67.6	69.9	71.0	73.4	69.2	72.5	80.4	81.9	73.6	76.0
	ECACL (ICCV'21)	75.3	79.0	74.1	77.3	75.3	79.4	65.0	70.6	72.1	74.6	68.1	71.6	79.7	82.4	72.8	76.4
	MCL (IJCAI'22)	77.4	79.4	74.6	76.3	75.5	78.8	66.4	70.9	74.0	74.7	70.7	72.3	82.0	83.3	74.4	76.5
	SLA (CVPR'23)	79.8	81.6	75.6	76.0	77.4	80.3	68.1	71.3	71.7	73.5	71.7	73.5	80.4	82.5	75.0	76.9
	EFTL (AAAI'24)	79.6	81.2	74.9	77.1	78.2	81.8	69.3	72.8	71.8	74.4	69.9	71.5	83.1	84.4	75.3	77.6
	FMLM (ECCV'24)	80.9	81.1	79.9	80.2	80.1	81.1	73.7	76.8	79.2	82.5	78.4	78.5	86.9	90.1	78.7	81.2
	🎓 GraDA (S)	**94.5**	**96.3**	**96.6**	**97.0**	**95.3**	**95.5**	**91.5**	**93.5**	**95.5**	**95.9**	**93.6**	**93.8**	**95.3**	**96.5**	**94.8**	**95.5**
ViT-B	🎓 GraDA (T)	95.2	97.0	97.1	97.7	96.0	96.2	92.1	94.2	96.1	96.5	94.4	94.5	96.6	97.3	95.4	96.2

Table 2: Accuracy (%) on **DomainNet** under the SSDA setting. The best results are marked as **bold**.

of **DomainNet** (Peng et al., 2019) includes 126 classes in 4 diverse domains: *real* (rel), *clipart* (clp), *painting* (pnt), and *sketch* (skt), where we follow previous works (Saito et al., 2019; Zhang & Lee, 2023) to verify our method on 7 DA tasks. More information is provided in the *Suppl. Material*.

Experimental Settings. All experiments were conducted on a single RTX-4090 GPU. For the feature extractor of the teacher network, we utilized ViT-B model with a 16×16 patch size, whereas the ResNet family (He et al., 2016) served as the feature extractor for the student network, similar to (Lu et al., 2020; Xiao et al., 2023). Each feature extractor was pre-trained on ImageNet-1k. For the classifier, GCN (Luo et al., 2020) was used to implement the CA module in the teacher network, while a two-layer MLP (Li et al., 2021a; Yu & Lin, 2023) was employed in the student network. Both networks were optimized using SGD with a learning rate and weight decay of 5×10^{-4}, and momentum of 0.9, respectively. We set the mini-batch size to $B = 32$ and the pseudo-label threshold in Eq. (7) to $\tau = 0.95$. Teacher and student networks are trained for $E = 100$ episodes, with $T = 500$ steps for **Office-Home** and $T = 1{,}000$ for **VisDA2017** and **DomainNet** per episode.

4.2 Comparison with State-of-the-Arts

Notably, the results of the student serve as a baseline for a fair comparison with prior CNN-based methods, while the results of the teacher are used solely for analysis.

UDA Methods. Tables 1a and 1b show the results on **VisDA2017** and **Office-Home**, respectively. Specifically, on **VisDA2017**, GraDA (S) and GraDA (T) achieve 96.5% and 97.0%, respectively, indicating a minimal performance gap between the student and teacher networks. Additionally, GraDA (S) outperforms the second-best method, HVCLIP Vesdapunt et al. (2024), with a gain of 6.5%. Under a fair comparison using the same ViT-B backbone, GraDA (T) also surpasses HVCLIP by 5.5%. On **Office-Home**, GraDA (S) still achieves the best results across all tasks, surpassing the DA method with KD, AML Zhou et al. (2023), in several challenging tasks, such as Ar→Cl, Pr→Cl, and Rw→Cl, with notable accuracies of 88.6%, 88.3%, and 90.9%, respectively. As a result, the mean accuracy of GraDA (S) reaches 93.8% across 12 DA tasks, improving by 14.3% compared to the second-best method, HVCLIP. Mean accuracy of GraDA (T) also achieves 94.0%, it surpasses all ViT-based competitors, and exceeds the second-best HVCLIP by 2.0%.

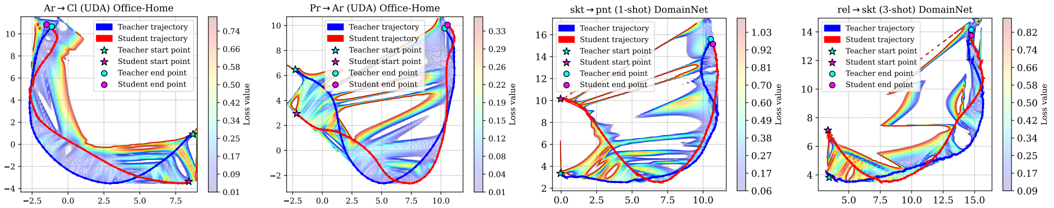

(a) *Art*→*Clipart* (UDA) (b) *Product*→*Art* (UDA) (c) *skt*→*pnt* (1-shot) (d) *rel*→*skt* (3-shot)

Figure 3: Convergence trajectory in the loss landscape of teacher and student networks.

Scenario		Settings	Office-Home (UDA) (ResNet50)	DomainNet (SSDA) (ResNet34)
			Student Mean Acc. (%)	
Vanilla **Student**	**S1**	Supervised	59.4	60.0
	S2	+ Self-Enhanced	62.7	71.3
	S3	+ $\mathcal{L}_{cc}^{S}(p_S(x_i^{tar}))$	69.1	73.4
With **Teacher**	**S4**	Supervised	84.0	87.1
	S5	+ Self-Enhanced	93.5	95.0
	S6	+ $\mathcal{L}_{cc}^{T}(p_T(x_i^{tar}))$	93.8	95.5

Table 3: Ablation study on **Office-Home** and **DomainNet** under UDA and 3-shot SSDA.

Teacher-Student Pair			rel→clp	clp→skt	skt→pnt	pnt→rel	Mean
P1	**T**	ResNet101+MLP	77.0	68.1	73.6	81.7	75.1
	S	ResNet34+MLP	76.8	67.6	73.3	81.3	74.8
P2	**T**	ViT-B+MLP	85.3	79.1	85.3	90.9	85.2
	S	ResNet34+MLP	85.3	78.6	85.1	89.6	84.7
P3	**T**	ResNet101+CA	95.1	90.5	93.0	91.8	92.6
	S	ResNet34+MLP	93.9	88.6	90.9	93.9	91.8
P4	**T**	ViT-B+CA	97.0	94.2	96.5	97.3	96.3
	S	ResNet34+MLP	96.3	93.5	95.9	96.5	95.6

Table 4: Performance of student (**S**) paired with various teachers (**T**) on **DomainNet** (3-shot).

SSDA Methods. Similar to Saito et al. (2019); Li et al. (2021a), we simply add a few labeled target samples (1-shot or 3-shot) into the training dataset under the SSDA setting. As listed in Table 2, GraDA (**S**) provides the remarkable results across 7 DA tasks on **DomainNet** with an average accuracy of 94.8% and 95.5% corresponding to the 1-shot and 3-shot settings, respectively. Moreover, the average accuracy gap between GraDA (**S**) and GraDA (**T**) is narrowed to 0.6% and 0.7% under the 1-shot and 3-shot, respectively. These results demonstrate that the student network, utilizing a *small* model (ResNet34), can efficiently capture the knowledge of the *larger* teacher network (ViT-B).

4.3 Analyses

As observed, in settings **S1**, **S2**, and **S3**, where the student network operates without guidance from the teacher network, it achieves maximum accuracies of only 69.1% and 73.4% on **Office-Home** and **DomainNet**, respectively. In contrast, with teacher guidance in settings **S4**, **S5**, and **S6**, the classification performance of the student network is significantly enhanced. Specifically, in setting **S4**, the student network's results improve by 14.9% and 13.7%, despite the limited quality and quantity of pseudo labels provided by the teacher network, as only intra-class relationships within the source domain are considered in Eq. (6). In setting **S5**, the teacher network improves generalization to unlabeled target data thanks to intra-class relationships, while class-aware feature alignment mitigates the domain shift issue using Eq. (9). Furthermore, setting **S6** overcomes the ambiguous class confusion using Eq. (10). As a result, the quality and quantity of pseudo labels from the teacher network increase, enhancing the student network's performance.

Teacher-Student Pair	#Params (M)	Ar→Cl	Cl→Pr	Pr→Rw	Rw→Ar	Mean
ResNet50+CA (**T**)	30.3	78.3	83.9	93.8	92.5	87.1
ResNet50+MLP (**S**)	24.6	77.8	83.8	93.5	92.3	86.9
ViT-tiny+CA (**T**)	8.1	68.7	81.4	93.0	87.5	82.7
ViT-tiny+MLP (**S**)	5.7	68.3	80.5	92.8	87.3	82.2
HVCLIP (ResNet50)	≈101.5	62.0	84.3	87.8	80.3	78.6

Table 5: Ablation study on various teacher-student pairs on **Office-Home** with UDA. (*Complete DA tasks in Suppl.*)

Can a Teacher Truly Educate a Student? To examine this, we use the gradient trajectory to observe the changes in the learning behavior of teacher and student networks with the pseudo label-based gradient guidance algorithm. We visualize the convergence trajectory of two UDA tasks on **Office-Home**: Ar→Cl and Pr→Ar (Fig. 3a), two SSDA tasks on **DomainNet**: skt→pnt and rel→skt with 1-shot and 3-shot settings (Fig. 3b), respectively. As shown in these figures, both the teacher and student models are initialized with random parameters, leading to different starting points. Nevertheless, the teacher network converges toward an optimal solution, followed by the student, ultimately aligning within a minimal region with a low loss value.

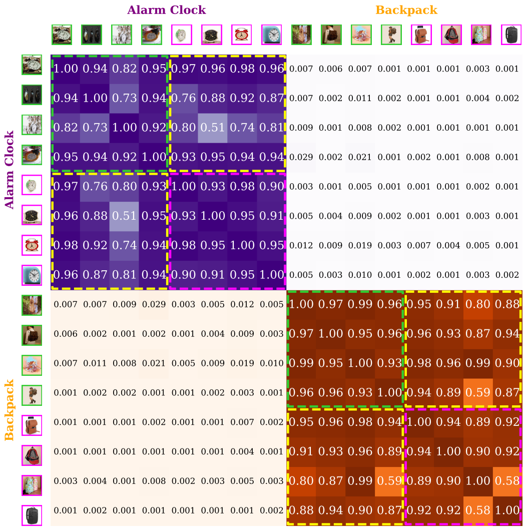

Figure 4: Illustration of category-level aggregation (similarity matrix $\tilde{S}$) of the UDA task Ar→Rw on **Office-Home**. Relationships between samples within the source and target domains are outlined in dashed green and pink boxes, respectively. Relationships of cross-domain samples are outlined by dashed yellow boxes.

Can a Student Perform Better with a Better Teacher? We verify the critical role of teacher network design in optimizing the effectiveness of the knowledge distillation scheme. Experiments are conducted using ResNet34+MLP as the anchor student network, paired with various types of teacher networks such as ResNet101+MLP, ViT-B+MLP, ResNet101+CA, and ViT-B+CA corresponding to **P1**, **P2**, **P3**, and **P4**, respectively. These teacher-student pairs are evaluated on 4 DA tasks within **DomainNet** under a 3-shot setting. As reported in Tab. 4, the results of **P2** significantly outperform those of **P1**, attributed to ViT-B's superior capacity for image representation compared to ResNet101. However, a comparison among **P1**, **P2**, and **P3** reveals a critical insight: the category-level aggregation (+CA) module proves to be a pivotal component in enhancing the effectiveness of knowledge distillation. The CA module not only facilitates improved intra-class generalization within source and target domains but also mitigates domain shift across these domains through class-aware feature alignment. Based on these findings, ViT-B+CA, associated with **P4**, is selected as the optimal teacher network, surpassing the other teacher networks and achieving the best accuracy of 96.3%. The classification performance of the student network in **P4** exceeds that of the student network in **P1**, including the least effective teacher network, by 20.8%.

Fairness of the Teacher Network. We conduct an ablation where the (**T**) and (**S**) networks share the same backbone on four **Office-Home** UDA tasks (Tab. 5). Even with identical ResNet50 or the smaller ViT-Tiny, GraDA still outperforms HVCLIP (Tab. 1b). This demonstrates that GraDA's gains stem from the proposed CA module and effective pseudo labels, not just the backbone.

Effectiveness of CA Module. The category-level aggregation (CA) mechanism plays a crucial role in the teacher network, which enhances *intra-class representations* within a domain and facilitates *class-aware alignment* across domains. To demonstrate this, we present Fig. 4, which visualizes the similarity matrix $\tilde{S}$ generated by the teacher network for a mini-batch ($B = 16$) in the Ar→Rw task, encompassing both source and target test samples. As shown, CA functions effectively, exhibiting high similarity among same-category samples, both within and across domains.

5 Conclusion

We introduce GraDA, a novel method designed to enhance student network performance in knowledge distillation for domain adaptation tasks. To achieve this, we first developed a strong teacher network by integrating a ViT backbone with a Category-level Aggregation (CA) module to produce robust representations. The CA module enhances the teacher's generalization ability by capturing *intra-class relations* within each domain and reducing domain shift between domains through *class-aware feature alignment*. We then proposed a gradient-guided knowledge distillation approach to optimize the transfer of knowledge from the ViT-based teacher to a lightweight CNN-based student, which is primarily used during inference. By providing high-quality pseudo labels, the ViT-based teacher guides the gradient updates of the student's parameters. Experiments across diverse settings demonstrate that GraDA significantly outperforms state-of-the-art methods on widely used benchmarks. Notably, this success is fully explainable, as evidenced by thorough qualitative analyses.

Limitation. While the CA module improves the teacher's generalization, aggregating features from noisy labels may introduce accumulated errors, degrading its quality and guidance to the student. It would be interesting to investigate incorporating a denoising module before the CA module.

REFERENCES

Hritam Basak and Zhaozheng Yin. Forget more to learn more: Domain-specific feature unlearning for semi-supervised and unsupervised domain adaptation. In *Eur. Conf. Comput. Vis.*, 2024.

Shai Ben-David, John Blitzer, Koby Crammer, Alex Kulesza, Fernando Pereira, and Jennifer Wortman Vaughan. A theory of learning from different domains. *Machine learning*, pp. 151–175, 2010.

Lucas Beyer, Xiaohua Zhai, Amélie Royer, Larisa Markeeva, Rohan Anil, and Alexander Kolesnikov. Knowledge distillation: A good teacher is patient and consistent. In *IEEE Conf. Comput. Vis. Pattern Recog.*, pp. 10925–10934, 2022.

Zhangjie Cao, Lijia Ma, Mingsheng Long, and Jianmin Wang. Partial adversarial domain adaptation. In *Eur. Conf. Comput. Vis.*, pp. 135–150, 2018.

Barbara Caputo, Henning Müller, Jesus Martinez-Gomez, Mauricio Villegas, Burak Acar, Novi Patricia, Neda Marvasti, Suzan Üsküdarlı, Roberto Paredes, Miguel Cazorla, et al. Imageclef 2014: Overview and analysis of the results. In *International Conference of the Cross-Language Evaluation Forum for European Languages*, pp. 192–211, 2014.

Lin Chen, Huaian Chen, Zhixiang Wei, Xin Jin, Xiao Tan, Yi Jin, and Enhong Chen. Reusing the task-specific classifier as a discriminator: Discriminator-free adversarial domain adaptation. In *IEEE Conf. Comput. Vis. Pattern Recog.*, pp. 7181–7190, 2022.

Pengguang Chen, Shu Liu, Hengshuang Zhao, and Jiaya Jia. Distilling knowledge via knowledge review. In *IEEE Conf. Comput. Vis. Pattern Recog.*, pp. 5008–5017, 2021.

Shuhao Cui, Shuhui Wang, Junbao Zhuo, Chi Su, Qingming Huang, and Qi Tian. Gradually vanishing bridge for adversarial domain adaptation. In *IEEE Conf. Comput. Vis. Pattern Recog.*, pp. 12455–12464, 2020.

Alexey Dosovitskiy, Lucas Beyer, Alexander Kolesnikov, Dirk Weissenborn, Thomas Unterthiner Xiaohua Zhai, Mostafa Dehghani, Matthias Minderer, Georg Heigold, Sylvain Gelly, Jakob Uszkoreit, and Neil Houlsby. An image is worth 16x16 words: Transformers for image recognition at scale. In *Int. Conf. Learn. Represent.*, 2021.

Zhekai Du, Xinyao Li, Fengling Li, Ke Lu, Lei Zhu, and Jingjing Li. Domain-agnostic mutual prompting for unsupervised domain adaptation. In *IEEE Conf. Comput. Vis. Pattern Recog.*, pp. 23375–23384, 2024.

Yaroslav Ganin, Evgeniya Ustinova, Hana Ajakan, Pascal Germain, Hugo Larochelle, François Laviolette, Mario Marchand, and Victor Lempitsky. Domain-adversarial training of neural networks. *Journal of Machine Learning Research*, 17(1):2096–2030, 2016.

Jiujun He, Bin Liu, and Guosheng Yin. Enhancing semi-supervised domain adaptation via effective target labeling. In *AAAI*, volume 38, pp. 12385–12393, 2024.

Kaiming He, Xiangyu Zhang, Shaoqing Ren, and Jian Sun. Deep residual learning for image recognition. In *IEEE Conf. Comput. Vis. Pattern Recog.*, pp. 770–778, 2016.

Byeongho Heo, Jeesoo Kim, Sangdoo Yun, Hyojin Park, Nojun Kwak, and Jin Young Choi. A comprehensive overhaul of feature distillation. In *Int. Conf. Comput. Vis.*, pp. 1921–1930, 2019.

Geoffrey Hinton. Distilling the knowledge in a neural network. *arXiv preprint arXiv:1503.02531*, 2015.

Tao Huang, Shan You, Fei Wang, Chen Qian, and Chang Xu. Knowledge distillation from a stronger teacher. In *Adv. Neural Inform. Process. Syst.*, volume 35, pp. 33716–33727, 2022.

Xinyang Huang, Chuang Zhu, and Wenkai Chen. Semi-supervised domain adaptation via prototype-based multi-level learning. In *IJCAI*, 2023.

Sergey Ioffe and Christian Szegedy. Batch normalization: Accelerating deep network training by reducing internal covariate shift. *arXiv preprint arXiv:1502.03167*, 2015.

Joonhyeok Jang, Sunhyeok Lee, Seonghak Kim, Jung-Un Kim, Seonghyun Kim, and Daeshik Kim. Robust unsupervised domain adaptation through negative-view regularization. In *Winter Conference on Applications of Computer Vision*, pp. 2462–2471, 2024.

Pin Jiang, Aming Wu, Yahong Han, Yunfeng Shao, Meiyu Qi, and Bingshuai Li. Bidirectional adversarial training for semi-supervised domain adaptation. In Christian Bessiere (ed.), *IJCAI*, pp. 934–940. International Joint Conferences on Artificial Intelligence Organization, 7 2020.

Ying Jin, Ximei Wang, Mingsheng Long, and Jianmin Wang. Minimum class confusion for versatile domain adaptation. In *Eur. Conf. Comput. Vis.*, pp. 464–480, 2020.

Osman Semih Kayhan and Jan C van Gemert. On translation invariance in cnns: Convolutional layers can exploit absolute spatial location. In *IEEE Conf. Comput. Vis. Pattern Recog.*, pp. 14274–14285, 2020.

Taekyung Kim and Changick Kim. Attract, perturb, and explore: Learning a feature alignment network for semi-supervised domain adaptation. In *Eur. Conf. Comput. Vis.*, pp. 591–607, 2020.

Thomas N Kipf and Max Welling. Semi-supervised classification with graph convolutional networks. In *Int. Conf. Learn. Represent.*, 2017.

Alex Krizhevsky, Ilya Sutskever, and Geoffrey E Hinton. Imagenet classification with deep convolutional neural networks. In *Adv. Neural Inform. Process. Syst.*, volume 25, 2012.

Da Li, Yongxin Yang, Yi-Zhe Song, and Timothy M. Hospedales. Deeper, broader and artier domain generalization. In *Int. Conf. Comput. Vis.*, Oct 2017.

Jichang Li, Guanbin Li, Yemin Shi, and Yizhou Yu. Cross-domain adaptive clustering for semi-supervised domain adaptation. In *IEEE Conf. Comput. Vis. Pattern Recog.*, pp. 2505–2514, 2021a.

Kai Li, Chang Liu, Handong Zhao, Yulun Zhang, and Yun Fu. Ecacl: A holistic framework for semi-supervised domain adaptation. In *Int. Conf. Comput. Vis.*, pp. 8578–8587, 2021b.

Shuang Li, Mixue Xie, Fangrui Lv, Chi Harold Liu, Jian Liang, Chen Qin, and Wei Li. Semantic concentration for domain adaptation. In *Int. Conf. Comput. Vis.*, pp. 9102–9111, 2021c.

Xinyi Liu, Tao Dai, Shu-Tao Xia, and Yong Jiang. Self-ensemble variance regularization for domain adaptation. In *ICASSP*, pp. 3853–3857. IEEE, 2022a.

Yufan Liu, Jiajiong Cao, Bing Li, Weiming Hu, Jingting Ding, and Liang Li. Cross-architecture knowledge distillation. In *Asian Conference on Computer Vision*, pp. 3396–3411, December 2022b.

Zhihe Lu, Yongxin Yang, Xiatian Zhu, Cong Liu, Yi-Zhe Song, and Tao Xiang. Stochastic classifiers for unsupervised domain adaptation. In *IEEE Conf. Comput. Vis. Pattern Recog.*, pp. 9111–9120, 2020.

Yadan Luo, Zijian Wang, Zi Huang, and Mahsa Baktashmotlagh. Progressive graph learning for open-set domain adaptation. In *Int. Conf. Mach. Learn.*, pp. 6468–6478. PMLR, 2020.

You-Wei Luo and Chuan-Xian Ren. Conditional bures metric for domain adaptation. In *IEEE Conf. Comput. Vis. Pattern Recog.*, pp. 13989–13998, 2021.

You-Wei Luo, Chuan-Xian Ren, Xiao-Lin Xu, and Qingshan Liu. Geometric understanding of discriminability and transferability for visual domain adaptation. *IEEE Trans. Pattern Anal. Mach. Intell.*, 2024.

Zong Martin, Qiu Zengyu, Ma Xinzhu, Yang Kunlin, Liu Chunya, Hou Jun, Yi Shuai, and Ouyang Wanli. Better teacher better student: Dynamic prior knowledge for knowledge distillation. In *Int. Conf. Learn. Represent.*, 2023.

Leland McInnes, John Healy, and James Melville. Umap: Uniform manifold approximation and projection for dimension reduction. *arXiv preprint arXiv:1802.03426*, 2018.

Jaemin Na, Heechul Jung, Hyung Jin Chang, and Wonjun Hwang. Fixbi: Bridging domain spaces for unsupervised domain adaptation. In *IEEE Conf. Comput. Vis. Pattern Recog.*, pp. 1094–1103, 2021.

Muhammad Muzammal Naseer, Kanchana Ranasinghe, Salman H Khan, Munawar Hayat, Fahad Shahbaz Khan, and Ming-Hsuan Yang. Intriguing properties of vision transformers. In *Adv. Neural Inform. Process. Syst.*, volume 34, pp. 23296–23308, 2021.

Ba Hung Ngo, Nhat-Tuong Do-Tran, Tuan-Ngoc Nguyen, Hae-Gon Jeon, and Tae Jong Choi. Learning cnn on vit: A hybrid model to explicitly class-specific boundaries for domain adaptation. In *IEEE Conf. Comput. Vis. Pattern Recog.*, pp. 28545–28554, June 2024.

Xingchao Peng, Ben Usman, Neela Kaushik, Dequan Wang, Judy Hoffman, and Kate Saenko. Visda: A synthetic-to-real benchmark for visual domain adaptation. In *IEEE Conf. Comput. Vis. Pattern Recog. Worksh.*, June 2018.

Xingchao Peng, Qinxun Bai, Xide Xia, Zijun Huang, Kate Saenko, and Bo Wang. Moment matching for multi-source domain adaptation. In *Int. Conf. Comput. Vis.*, October 2019.

Viraj Prabhu, Shivam Khare, Deeksha Kartik, and Judy Hoffman. Sentry: Selective entropy optimization via committee consistency for unsupervised domain adaptation. In *Int. Conf. Comput. Vis.*, pp. 8558–8567, 2021.

Can Qin, Lichen Wang, Qianqian Ma, Yu Yin, Huan Wang, and Yun Fu. Contradictory structure learning for semi-supervised domain adaptation. In *Proceedings of the 2021 SIAM International Conference on Data Mining (SDM)*, pp. 576–584. SIAM, 2021.

Adriana Romero, Nicolas Ballas, Samira Ebrahimi Kahou, Antoine Chassang, Carlo Gatta, and Yoshua Bengio. Fitnets: Hints for thin deep nets. In *Int. Conf. Learn. Represent.*, 2015.

Kate Saenko, Brian Kulis, Mario Fritz, and Trevor Darrell. Adapting visual category models to new domains. In *Eur. Conf. Comput. Vis.*, pp. 213–226. Springer, 2010.

Kuniaki Saito, Kohei Watanabe, Yoshitaka Ushiku, and Tatsuya Harada. Maximum classifier discrepancy for unsupervised domain adaptation. In *IEEE Conf. Comput. Vis. Pattern Recog.*, 2018.

Kuniaki Saito, Donghyun Kim, Stan Sclaroff, Trevor Darrell, and Kate Saenko. Semi-supervised domain adaptation via minimax entropy. In *Int. Conf. Comput. Vis.*, pp. 8050–8058, 2019.

Ramprasaath R Selvaraju, Michael Cogswell, Abhishek Das, Ramakrishna Vedantam, Devi Parikh, and Dhruv Batra. Grad-cam: Visual explanations from deep networks via gradient-based localization. In *Int. Conf. Comput. Vis.*, pp. 618–626, 2017.

Ayan Sengupta, Shantanu Dixit, Md Shad Akhtar, and Tanmoy Chakraborty. A good learner can teach better: Teacher-student collaborative knowledge distillation. In *Int. Conf. Learn. Represent.*, 2024.

Ankit Singh. Clda: Contrastive learning for semi-supervised domain adaptation. In *Adv. Neural Inform. Process. Syst.*, pp. 5089–5101, 2021.

Kihyuk Sohn, David Berthelot, Nicholas Carlini, Zizhao Zhang, Han Zhang, Colin A Raffel, Ekin Dogus Cubuk, Alexey Kurakin, and Chun-Liang Li. Fixmatch: Simplifying semi-supervised learning with consistency and confidence. In *Adv. Neural Inform. Process. Syst.*, pp. 596–608, 2020.

Tao Sun, Cheng Lu, Tianshuo Zhang, and Haibin Ling. Safe self-refinement for transformer-based domain adaptation. In *IEEE Conf. Comput. Vis. Pattern Recog.*, pp. 7191–7200, 2022.

Charlene Tan and Diwi Binti Abbas. The'teach less, learn more'initiative in singapore: New pedagogies for islamic religious schools? *KEDI Journal of Educational Policy*, 2009.

Laurens Van der Maaten and Geoffrey Hinton. Visualizing data using t-sne. *Journal of Machine Learning Research*, 9(11), 2008.

Hemanth Venkateswara, Jose Eusebio, Shayok Chakraborty, and Sethuraman Panchanathan. Deep hashing network for unsupervised domain adaptation. In *IEEE Conf. Comput. Vis. Pattern Recog.*, July 2017.

Noranart Vesdapunt, Kah Kuen Fu, Yue Wu, Xu Zhang, and Pradeep Natarajan. Hvclip: High-dimensional vector in clip for unsupervised domain adaptation. In *Eur. Conf. Comput. Vis.*, 2024.

Lean Wang, Lei Li, and Xu Sun. Gradient knowledge distillation for pre-trained language models. In *Adv. Neural Inform. Process. Syst.*, 2022.

Thomas Westfechtel, Hao-Wei Yeh, Qier Meng, Yusuke Mukuta, and Tatsuya Harada. Backprop induced feature weighting for adversarial domain adaptation with iterative label distribution alignment. In *Winter Conference on Applications of Computer Vision*, pp. 392–401, 2023.

Thomas Westfechtel, Hao-Wei Yeh, Dexuan Zhang, and Tatsuya Harada. Gradual source domain expansion for unsupervised domain adaptation. In *Winter Conference on Applications of Computer Vision*, pp. 1946–1955, 2024.

Zhiqing Xiao, Haobo Wang, Ying Jin, Lei Feng, Gang Chen, Fei Huang, and Junbo Zhao. Spa: a graph spectral alignment perspective for domain adaptation. In *Adv. Neural Inform. Process. Syst.*, volume 36, 2023.

Tongkun Xu, Weihua Chen, Pichao Wang, Fan Wang, Hao Li, and Rong Jin. Cdtrans: Cross-domain transformer for unsupervised domain adaptation. In *Int. Conf. Learn. Represent.*, 2022.

Zizheng Yan, Yushuang Wu, Guanbin Li, Yipeng Qin, Xiaoguang Han, and Shuguang Cui. Multi-level consistency learning for semi-supervised domain adaptation. In *IJCAI*, 2022.

Jinyu Yang, Jingjing Liu, Ning Xu, and Junzhou Huang. Tvt: Transferable vision transformer for unsupervised domain adaptation. In *Winter Conference on Applications of Computer Vision*, pp. 520–530, 2023.

Luyu Yang, Yan Wang, Mingfei Gao, Abhinav Shrivastava, Kilian Q. Weinberger, Wei-Lun Chao, and Ser-Nam Lim. Deep co-training with task decomposition for semi-supervised domain adaptation. In *Int. Conf. Comput. Vis.*, pp. 8906–8916, 2021.

Yu-Chu Yu and Hsuan-Tien Lin. Semi-supervised domain adaptation with source label adaptation. In *IEEE Conf. Comput. Vis. Pattern Recog.*, pp. 24100–24109, 2023.

Can Zhang and Gim Hee Lee. Get: Generative target structure debiasing for domain adaptation. In *Int. Conf. Comput. Vis.*, pp. 23577–23588, 2023.

Xinyu Zhang, Meng Kang, and Shuai Lü. Low category uncertainty and high training potential instance learning for unsupervised domain adaptation. In *AAAI*, pp. 16881–16889, 2024.

Borui Zhao, Quan Cui, Renjie Song, Yiyu Qiu, and Jiajun Liang. Decoupled knowledge distillation. In *IEEE Conf. Comput. Vis. Pattern Recog.*, pp. 11953–11962, 2022.

Lihua Zhou, Siying Xiao, Mao Ye, Xiatian Zhu, and Shuaifeng Li. Adaptive mutual learning for unsupervised domain adaptation. *IEEE Transactions on Circuits and Systems for Video Technology*, 33(11):6622–6634, 2023.

Jinjing Zhu, Haotian Bai, and Lin Wang. Patch-mix transformer for unsupervised domain adaptation: A game perspective. In *IEEE Conf. Comput. Vis. Pattern Recog.*, pp. 3561–3571, 2023a.

Jinjing Zhu, Yunhao Luo, Xu Zheng, Hao Wang, and Lin Wang. A good student is cooperative and reliable: Cnn-transformer collaborative learning for semantic segmentation. In *Int. Conf. Comput. Vis.*, pp. 11720–11730, October 2023b.

A Appendix

This *Supplementary Material* provides five-fold information. First, we summarize the notations frequently used in the main manuscript and their corresponding definitions (Sec. B) and a detailed overview of all datasets (Sec. C). Second, a concise pseudocode for GraDA is included for clarity (Sec. D), and the implementation details of the teacher and student networks are thoroughly explained (Sec. E). Third, additional results in the UDA and SSDA settings are presented in Sec. F. Fourth, various aspects are discussed in more detail, including the diversity of student networks in GraDA, the pivotal role of CA in teacher network design, and the influence of CA on student performance through pseudo-label generation, supported by additional results and discussion (Sec. G). Finally, qualitative results using t-SNE and Grad-CAM are provided to further visually evaluate GraDA (Sec. H). Below, we present the table of contents to facilitate easy access to the information.

Contents

	Notation	Definition
Abbreviation	DA	Domain Adaptation
	UDA	Unsupervised Domain Adaptation
	SSDA	Semi-supervised Domain Adaptation
	KD	Knowledge Distillation
	CNN	Convolutional Neural Networks
	ViT	Vision Transformer
	MLP	Multilayer Perceptron
	CA	Category-level Aggregation
	GCN	Graph Convolutional Networks
Symbol in **Data Setting**	D_{src}	Set of the labeled source domain
	x_i^{src}	The i-th image from the source domain
	y_i^{src}	Label of the source image x_i^{src}
	N_{src}	The number of samples in the source domain
	D_{tar}	Set of the unlabeled target domain
	x_i^{tar}	The i-th image from the target domain
	y_i^{tar}	Label of the target image x_i^{tar}
	N_{tar}	The number of samples in the target dataset
	C	Number of categories in both domains
	D_{ps}^e	Pseudo-labeled set generated at episode e
	$\hat{y}_i^{ps}$	Pseudo label for the target image x_i^{tar}
	N_{ps}	The number of samples in the pseudo-labeled set
	D_{cb}^e	Combined dataset at episode e of D_{src} and D_{ps}^e
	x_i^{cb}	The i-th image from the combined set
	y_i^{cb}	Label of the combined image x_i^{cb}
	N_{cb}	The number of samples in the combined set
Symbol in **Train.**	η	Learning rate of the teacher and student networks
	τ	Confidence threshold for pseudo-label generation
	B	The number of samples in a mini-batch
	E	The number of training episodes
	e	Episode index in the training process
	T	Number of training steps per episode

	Notation	Definition
Symbol in **Teacher**	f_{vit}	ViT-based feature extractor
	f_{sim}	Similarity network in the CA module
	f_{agg}	Category aggregation network in the CA module
	θ_{vit}	Set of learnable parameters for f_{vit}
	θ_{sim}	Set of learnable parameters for f_{sim}
	θ_{agg}	Set of learnable parameters for f_{agg}
	z_i^{vit}	Feature vector generated by f_{vit} for sample x_i
	d	Embedding size of the feature vector z_i^{vit}
	$\hat{s}_{i,j}$	Similarity score between feature vectors
	$\hat{S}$	Similarity matrix within a mini-batch B
	$\tilde{s}_{i,j}$	Normalized similarity score
	$\tilde{S}$	Normalized similarity matrix
	I	Identity matrix used for normalization
	D	Degree matrix of $\hat{S} + I$
	z_i^T	Aggregated feature vector
	$p_T(x_i)$	Prediction of the teacher network for sample x_i
	$e_{i,j}$	Ground-truth of edge between two samples
	$\mathcal{L}_{bce}^T$	Binary cross-entropy loss of the teacher network
	$\mathcal{L}_{ce}^T$	Cross-entropy loss of the teacher network
	$\mathcal{L}_{cc}$	Cross-class confusion loss of the teacher network
Symbol in **Student**	f_{cnn}	CNN-based feature extractor
	MLP	MLP classifier
	θ_{cnn}	Set of learnable parameters for f_{cnn}
	θ_{mlp}	Set of learnable parameters for the MLP
	z_i^{cnn}	Feature vector generated by f_{cnn} for sample x_i
	d'	Embedding size of the feature vector z_i^{cnn}
	$p_S(x_i)$	Prediction of the student network for sample x_i
	$\mathcal{L}_{ce}^S$	Cross-entropy loss of the student network
	∇_{θ_S}	The gradient of the loss $\mathcal{L}_{ce}^S$ with respect to θ_S

Table 6: Abbreviation and symbol notation (**Train.** stands for Training).

B Notations

We summarize notations and their definitions frequently used in the proposed method, as listed in Tab. 6.

C Dataset Details

Table 7 provides an overview of popular domain adaptation datasets, including **VisDA2017**, **Office-Home**, **DomainNet**, **Office-31**, and **ImageCLEF-DA**. It details the number of categories and the number of images for each dataset, along with sample images from different domains.

VisDA2017 Peng et al. (2018) exhibits a significant domain gap when transferring from the *Synthetic* domain to the *Real-world* domain. It includes $152,397$ *Synthetic* images as the source domain and $55,388$ *Real-world* images as the target domain. Each domain consists of 12 different categories. The synthetic images are generated from 3D models, while the real images are collected from natural scenes.

Office-Home Venkateswara et al. (2017) contains approximately $15,500$ images across 65 categories from 4 distinct domains: *Art* (Ar), *Clipart* (Cl), *Product* (Pr), and *Real-World* (Rw). These 4 domains establish 12 cross-domain tasks: Ar→Cl, Ar→Pr, Ar→Rw, Cl→Ar, Cl→Pr, Cl→Rw, Pr→Ar, Pr→Cl, Pr→Rw, Rw→Ar, Rw→Cl, and Rw→Pr.

DomainNet Peng et al. (2019) contains approximately $600,000$ images from six domains: *clipart* (clp), *infograph* (inf), painting (pnt), *quickdraw* (qdw), *real* (rel), and *sketch* (skt). It includes 345 categories. In the SSDA setting, we use a subset with 126 classes across these domains to consistency with the prior SSDA works Saito et al. (2019); Qin et al. (2021); Yu & Lin (2023); Huang et al. (2023). In the UDA setting, we employ **Mini-DomainNet** as used in Prabhu et al. (2021); Westfechtel et al. (2023), a curated subset with 40 frequently observed classes across the same 4 domains, encompassing all 12 possible domain shifts.

Algorithm 1: Pseudocode of GraDA

```
1  Input: Source and target datasets: $D_{src} = \{(x_i^{src}, y_i^{src})\}_{i=1}^{N_{src}}$; $D_{tar} = \{x_i^{tar}\}_{i=1}^{N_{tar}}$;
2  Training Configuration: Threshold $\tau$, Total episodes $E$, training steps $T$, Mini-batch size $B$,
     Learning rate $\eta$
3  Initialization: Combined dataset $D_{cb}^0 \leftarrow D_{src}$
4  Network Architectures:
5      Teacher network: $f_{vit}$, $f_{sim}$ and $f_{agg}$. Set of parameters: $\theta_T = \{\theta_{vit}, \theta_{sim}, \theta_{agg}\}$
6      Student network: $f_{cnn}$ and MLP. Set of parameters: $\theta_S = \{\theta_{cnn}, \theta_{mlp}\}$;
7  ➤ TRAINING: for $e = 1$ to $E$ do
8      for $t = 1$ to $T$ do
9          Sample $\{(x_i^{cb}, y_i^{cb})\}_{i=1}^{B} \in D_{cb}^e$
10         • Training Strategy for the Teacher Network:
11         $\{z_i^{vit}\}_{i=1}^{B} \leftarrow \{f_{vit}(x_i^{cb}; \theta_{vit})\}_{i=1}^{B}$
12         ◇ Initialize similarity matrix: $\hat{S} \in \mathbb{R}^{B \times B}$
13         for $(i, j)$ in $(1..B, 1..B)$ do
14             ◇ Computing the $(i, j)$-th similarity score:
15             $\hat{s}_{i,j} \leftarrow \texttt{sigmoid}\big(f_{sim}(\|z_i^{vit} - z_j^{vit}\|; \theta_{sim})\big)$ where $\hat{s}_{i,j} \in \hat{S}$      ▷ Eq. (1).
16         $\tilde{S} \leftarrow D^{-\frac{1}{2}}(\hat{S} + I)D^{-\frac{1}{2}}$      ▷ Eq. (2).
17         for $i = 1$ to $B$ do
18             $z_i^T \leftarrow f_{agg}\Big(\big[z_i^{vit}, \sum_{j \in B} \tilde{s}_{i,j} \cdot z_j^{vit}\big]; \theta_{agg}\Big)$
19                 ▷ Eq. (3).
20             $p_T(x_i^{cb}) \leftarrow \texttt{softmax}(z_i^T)$
21         $\theta_T \leftarrow \theta_T - \eta \nabla_{\theta_T}(\mathcal{L}_{bce}^T + \mathcal{L}_{ce}^T + \mathcal{L}_{cc})$
22             ▷ $\mathcal{L}_{bce}^T$, $\mathcal{L}_{ce}^T$ and $\mathcal{L}_{cc}$ are computed in Eq. (4), Eq. (5) and Eq. (10), respectively.
23         • Training Strategy for Student Network: $z_i^{cnn} \leftarrow f_{cnn}(x_i^{cb}; \theta_{cnn})$
24         $p_S(x_i) \leftarrow \texttt{softmax}(\text{MLP}(z_i^{cnn}; \theta_{mlp}))$
25         $\theta_S \leftarrow \theta_S - \eta \nabla_{\theta_S} \mathcal{L}_{ce}^S$
26             ▷ $\mathcal{L}_{ce}^S$ is computed in Eq. (11).
27     ◇ Pseudo Label Generation: $D_{ps}^e \leftarrow \emptyset$
28     for $\{(x_i^{tar})\}_{i=1}^{B}$ in $D_{tar}$ do
29         $\{z_i^{vit}\}_{i=1}^{B} \leftarrow \{f_{vit}(x_i^{tar}; \theta_{vit})\}_{i=1}^{B}$
30         Repeat lines 13–20 to obtain $\{z_i^T\}_{i=1}^{B}$
31         for $i = 1$ to $B$ do
32             $p_T(x_i^{tar}) \leftarrow \texttt{softmax}(z_i^T)$
33             if $\texttt{max}\big(p_T(x_i^{tar})\big) \geq \tau$ then
34                 $\hat{y}_i^{ps} \leftarrow \texttt{argmax}\big(p_T(x_i^{tar})\big)$
35                     ▷ Assign pseudo label.
36                 $D_{ps}^e \leftarrow D_{ps}^e \cup \{(x_i^{tar}, \hat{y}_i^{ps})\}$
37                     ▷ Update pseudo-labeled set.
38     ◇ Update the combined set: $D_{cb}^e \leftarrow D_{src} \cup D_{ps}^e$
39 ➤ TESTING: $p_S(x_i^{tar}) \leftarrow \texttt{softmax}\big(\text{MLP}(f_{cnn}(x_i^{tar}))\big)$
40     ▷ Only the student network is used for testing.
```

Office-31 Saenko et al. (2010) contains $4,110$ images across 31 categories from three distinct domains: *Amazon* (A), *Webcam* (W), and *DSLR* (D). The *Amazon* domain consists of images from online merchants, *Webcam* includes low-resolution images taken by web cameras, and *DSLR* contains high-resolution images captured with a digital SLR camera. In UDA, all 6 possible domain adaptation tasks between these domains are considered: A→W, A→D, W→A, W→D, D→A, and D→W. In the SSDA setting, 2 tasks are evaluated: W→A and D→A.

Domain Adaptation Datasets					
VisDA2017: 12 categories		**Office-Home**: 65 categories			
Synthetic 152, 397 images	*Real-world* 55, 388 images	*Art* 2, 427 images	*Clipart* 4, 365 images	*Product* 4, 439 images	*Real-World* 4, 357 images
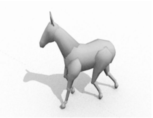			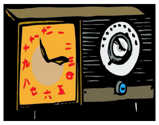		
DomainNet: 345 categories					
clipart 48, 837 images	*infograph* 53, 201 images	*painting* 75, 759 images	*quickdraw* 172, 500 images	*real* 175, 327 images	*sketch* 70, 386 images
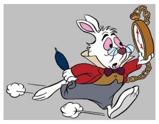					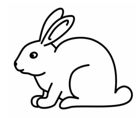
Office-31: 31 categories			**ImageCLEF-DA**: 12 categories		
Amazon 2, 817 images	*Webcam* 795 images	*DSLR* 498 images	*Caltech-256* 600 images	*ImageNet ILSVRC* 600 images	*Pascal VOC 2012* 600 images

Table 7: Overview of popular domain adaptation datasets, including **VisDA2017**, **Office-Home**, **DomainNet**, **Office-31**, and **ImageCLEF-DA**. The number of images reflects the scale of each dataset, while the example images per domain highlight the distribution discrepancy.

Net	Method	aero	bicycle	bus	car	horse	knife	motor	person	plant	skate	train	truck	Mean
ResNet101	MCC (ECCV'20)	88.1	80.3	80.5	71.5	90.1	93.2	85.0	71.6	89.4	73.8	85.0	36.9	78.8
	STAR (CVPR'20)	95.0	84.0	84.6	73.0	91.6	91.8	85.9	78.4	94.4	84.7	87.0	42.2	82.7
	FixBi (CVPR'21)	96.1	87.8	90.5	**90.3**	96.8	95.3	92.8	88.7	97.2	94.2	90.9	25.7	87.2
	DAMP (CVPR'24)	97.3	91.6	89.1	76.4	97.5	94.0	92.3	84.5	91.2	88.1	91.2	67.0	88.4
	HVCLIP (ECCV'24)	98.8	90.1	90.8	82.2	97.3	95.5	91.8	82.9	94.9	92.8	92.2	70.8	90.0
	🎓 GraDA (S)	**99.9**	**98.6**	**96.4**	88.4	**100.0**	**99.8**	**99.3**	**97.5**	**100.0**	**100.0**	**99.2**	**78.7**	**96.5**
ViT-B	PMTrans (CVPR'23)	98.9	93.7	84.5	73.3	99.0	98.0	96.2	67.8	94.2	98.4	96.6	49.0	87.5
	SSRT (CVPR'22)	98.9	87.6	89.1	84.8	98.3	98.7	96.3	81.1	94.9	97.9	94.5	43.1	88.8
	DAMP (CVPR'24)	98.7	92.8	91.7	80.1	98.9	96.9	94.9	83.2	93.9	94.9	94.8	70.2	90.9
	NVC (WACV'24)	98.5	89.0	88.5	92.0	98.5	98.3	96.2	88.4	98.5	97.9	95.0	55.4	91.4
	HVCLIP (ECCV'24)	99.0	93.7	92.1	84.5	98.8	96.2	94.2	88.6	96.9	96.7	94.5	74.4	92.5
	🎓 GraDA (T)	**100.0**	**99.1**	**97.9**	**89.4**	**100.0**	**100.0**	**99.7**	**98.5**	**100.0**	**99.9**	**99.9**	**79.5**	**97.0**

Table 8: Accuracy (%) on **VisDA2017** under the UDA setting. GraDA (**S**) and GraDA (**T**) are the student and teacher networks, respectively. For a fair comparison, we use GraDA (**S**) to compare with the prior CNN-based works, while the comparison of the teacher GraDA (**T**) and ViT-based DA works is provided for reference. The best classification accuracy is marked as **bold**.

ImageCLEF-DA Caputo et al. (2014) includes images from three domains: *Caltech-256* (C), *ImageNet ILSVRC 2012* (I), and *Pascal VOC 2012* (P). Each domain contains 12 categories with 50 images per category, totaling 600 images per domain. The dataset defines 6 domain adaptation tasks between these domains: I→P, P→I, I→C, C→I, C→P, and P→C.

D Pseudocode of GraDA

We provide the pseudocode of GraDA presented in Algorithm 1, which is straightforward and helps to gain a better understanding of GraDA. Note that the losses for the teacher network including $\mathcal{L}_{bce}^{T}$, $\mathcal{L}_{ce}^{T}$, and $\mathcal{L}_{cc}$, are specified in Eqs. 4, 5 and 10, respectively. Meanwhile, the loss $\mathcal{L}_{ce}^{S}$ for the student network is detailed in Eq. 11.

Net	Method	rel→clp	rel→pnt	rel→skt	clp→rel	clp→pnt	clp→skt	pnt→rel	pnt→clp	pnt→skt	skt→rel	skt→clp	skt→pnt	Mean
ResNet50	MCD (CVPR’18)	62.0	69.3	56.3	79.8	56.6	53.7	83.4	58.3	61.0	81.7	56.3	66.8	65.4
	PADA (ECCV’18)	65.9	67.1	58.4	74.7	53.1	52.9	79.8	59.3	57.9	76.5	67.0	61.1	64.5
	BIWAA-I (WACV’23)	79.9	75.2	75.4	87.9	72.1	75.7	88.9	77.8	76.7	88.8	80.5	74.5	79.4
	SENTRY (ICCV’21)	83.9	76.7	74.4	90.6	76.0	79.5	90.3	82.9	75.6	90.4	82.4	74.0	81.4
	LUHP (AAAI’24)	79.6	82.8	79.3	91.1	79.7	76.5	90.2	77.2	76.7	91.2	80.3	79.5	82.0
	GSDE (WACV’24)	82.9	79.2	80.8	91.9	78.2	80.0	90.9	84.1	79.2	90.3	83.4	76.1	83.1
	ECB (CVPR’24)	84.7	83.8	79.7	91.6	84.0	82.5	91.0	83.2	79.2	86.1	82.9	81.6	84.2
	🎓 GraDA (S)	**93.1**	**94.8**	**85.7**	**98.4**	**95.0**	**91.5**	**97.3**	**86.6**	**89.3**	**95.7**	**93.1**	**96.4**	**93.1**
ViT-B	🎓 GraDA (T)	93.4	95.0	86.2	98.7	95.5	91.9	98.2	86.9	90.0	96.4	93.4	96.7	93.5

Table 9: Accuracy (%) on **Mini-DomainNet** under the UDA setting. The best classification accuracy is marked as **bold**.

Net	Method	A→W	D→W	W→D	A→D	D→A	W→A	Mean
ResNet50	GVB-GD (CVPR’20)	94.8	98.7	100.0	95.0	73.4	73.7	89.3
	SCDA (ICCV’21)	94.2	98.7	99.8	95.2	75.7	76.2	90.0
	DALN (CVPR’22)	95.2	99.1	100.0	95.4	76.4	76.5	90.4
	BIWAA-I (WACV’23)	95.6	99.0	100.0	94.4	75.9	77.3	90.5
	GeT (ICCV’23)	95.4	99.1	100.0	95.4	76.6	77.0	90.6
	LUHP (AAAI’24)	94.2	98.6	100.0	95.2	77.7	78.6	90.7
	FixBi (CVPR’21)	96.1	99.3	100.0	95.0	78.7	79.4	91.4
	SPA (NIPS’23)	97.2	99.0	99.8	95.0	78.0	79.4	91.4
	HVCLIP (ECCV’24)	96.2	**99.4**	100.0	96.0	80.1	80.6	92.1
	🎓 GraDA (S)	**98.6**	99.3	**100.0**	**99.2**	**90.0**	**91.8**	**96.5**
ResNet34	🎓 GraDA (S)	99.3	99.4	100.0	99.2	90.8	91.4	96.7
ResNet18	🎓 GraDA (S)	98.5	99.3	100.0	98.8	90.0	91.3	96.3
ViT-B	🎓 GraDA (T)	99.4	100.0	100.0	99.2	90.7	92.1	96.9

Table 10: Accuracy (%) on **Office-31** under the UDA setting with various versions of ResNet, such as ResNet50, ResNet34, and ResNet18. The best classification accuracy is marked as **bold**.

E GRADA ARCHITECTURE

This section thoroughly provides detailed implementations of teacher and student network architectures.

E.1 TEACHER NETWORK

Feature Extractor. ViT-B Dosovitskiy et al. (2021) is adopted as the feature extractor f_{vit}, dividing the input image x_i into patches of size 16×16. After processing by the patch embedding network, a sequence of 144 patch tokens is obtained, with the `[CLS]` token added at the beginning. The sequence then passes through a stack of 12 transformer blocks, each comprising multi-head self-attention and a feedforward layer, with each followed by a normalization layer. A skip connection is applied between the input and output of the multi-head self-attention module. The `[CLS]` token obtained from the final transformer block is used as the feature vector $z_i^{vit} \in \mathbb{R}^d$, where $d = 768$. Given a batch of images with size B, it is processed by f_{vit} to produce a batch of feature vectors $\{z_i^{vit}\}_{i=1}^{B}$, which are then processed by the CA module to produce the aggregated feature vector z_i^T.

CA Module. Our CA module includes a similarity network f_{sim} and an aggregation network f_{agg}. For f_{sim}, we implement two convolutional layers: the first layer has the same input and output channels, which are 768, while the second layer projects from 768 to 1, *i.e.*, a scalar value for the similarity score. Batch Normalization Ioffe & Szegedy (2015) followed by a LeakyReLU activation is applied between these two convolutional layers. For f_{agg}, three convolutional layers are employed, each followed by Batch Normalization and LeakyReLU. The first two layers have the same input and output channels, which are 768, while the last one produces C logits, where C is the number of categories.

E.2 Student Network

Feature Extractor. The ResNet family He et al. (2016) and AlexNet Krizhevsky et al. (2012) are adopted as feature extractors for the student network, *i.e.*, f_{cnn}. The ResNet architectures used in this study include ResNet101, ResNet50, ResNet34, and ResNet18. The specific network applied to the student network depends on the dataset and settings to ensure a fair comparison with existing studies or for evaluation purposes. Given an input image x_i, the feature extractor f_{cnn} produces a feature vector $z_i^{cnn} \in \mathbb{R}^{d'}$, where d' represents the dimensionality of the feature vector. The value of d' depends on the specific feature extractor used: $d' = 512$ for ResNet18 and ResNet34, $d' = 2048$ for ResNet50 and ResNet101, and $d' = 4096$ for AlexNet.

MLP Classifier. The MLP classifier includes two linear layers. The first layer projects from a d' dimension to 512, and the second layer projects from 512 to C logits. Between the two linear layers, there is a normalization operation.

E.3 Comparison Between CA and MLP

We further highlight the differences between CA and MLP and analyze some significant time complexities. For a batch of B samples, CA constructs a similarity matrix $\tilde{S} \in \mathbb{R}^{B\times B}$, using f_{sim} for scoring and f_{agg} for feature aggregation and logits generation. Constructing the similarity matrix requires computing all possible pairwise feature differences in the batch, with a time complexity of $\mathcal{O}(B^2 \cdot d)$, where d is the feature vector dimension of f_{vit}. f_{sim} then assigns scalar similarity scores. Subsequently, feature aggregation involves a weighted sum of each feature vector with all others, costing $\mathcal{O}(B^2 \cdot d)$, followed by concatenation ($\mathcal{O}(B \cdot d)$) and f_{agg} to produce C-dimensional logits. In this manner, **the CA module projects aggregated feature vectors into the logit space**. In contrast, **the MLP generates the logits for each feature vector independently using a single network**. Although the proposed CA module introduces higher complexity, it is used only during training, whereas MLP integrated with CNN-based networks is used during inference, ensuring practicality.

F Additional Results

This section presents extensive experimental results on UDA and SSDA settings.

F.1 Unsupervised Domain Adaptation

VisDA2017. The classification accuracy for each class is listed in Tab. 8. Using ResNet101 as the backbone, the proposed student network GraDA (**S**) achieves the highest classification accuracy across all classes except for the "*car*" class. The average accuracy over the 12 classes for the student network reaches 96.5%, representing a 6.5% improvement over the second-best method, HVCLIP Vesdapunt et al. (2024). Compared to prior works using ViT-B as a backbone, the teacher network GraDA (**T**) also achieves the best accuracy of 97.0%. Notably, the mean accuracy gap between the student and teacher networks is marginal, measuring only 0.5%.

Mini-DomainNet. We reported the classification results of 12 DA tasks in Tab. 9. The average accuracy is 93.1%, surpassing the second-best method, ECB Ngo et al. (2024), by 8.9%.

Office-31 & **ImageCLEF-DA.** Tables 10 and 11 present the classification results for **Office-31** and **ImageCLEF-DA**, respectively. The proposed student model, utilizing ResNet50, achieves competitive accuracy on both datasets, with 96.5% on **Office-31** and 94.8% on **ImageCLEF-DA**.

F.2 Semi-supervised Domain Adaptation (SSDA)

The proposed method can be easily extended to the SSDA setting, where a limited number of labeled target samples per class are available, $D_{tar}^l = \{(x_i^{tar}, y_i^{tar})\}_{i=1}^{N_{tar}^l}$, where N_{tar}^l is the number of labeled target samples and $N_{tar}^l \ll N_{tar}$. We simply add D_{tar}^l into D_{cb}, which can be formed as follows:

$$D_{cb} = D_{src} \cup D_{ps} \cup D_{tar}^l, N_{cb} = N_{src} + N_{ps} + N_{tar}^l.$$

Net	Method	I→P	P→I	I→C	C→I	C→P	P→C	Mean
ResNet50	MCD (CVPR'18)	77.3	89.2	92.7	88.2	71.0	92.3	85.1
	GVB-GD (CVPR'20)	78.2	92.7	96.5	91.5	78.2	95.0	88.7
	VRDA (ICASSP'22)	78.3	93.8	96.3	93.5	78.0	96.3	89.4
	DALN (CVPR'22)	80.5	93.8	97.5	92.8	78.3	95.0	89.7
	CKB (CVPR'21)	80.7	93.7	97.0	93.5	79.2	97.0	90.2
	AML (IEEE Trans'23)	80.8	93.8	97.7	93.2	80.2	98.2	90.7
	GOAL (TPAMI'24)	82.2	94.1	97.3	95.6	82.3	96.4	91.3
	🎓 GraDA (S)	**85.8**	**99.5**	**99.5**	**99.3**	**84.8**	**99.8**	**94.8**
ResNet34	🎓 GraDA (S)	85.8	99.3	99.5	99.3	84.7	99.7	94.7
ResNet18	🎓 GraDA (S)	84.6	99.7	99.7	99.5	84.8	99.0	94.6
ViT-B	🎓 GraDA (T)	86.8	99.8	100.0	99.8	87.2	100.0	95.6

Table 11: Accuracy (%) on **ImageCLEF-DA** under UDA with various versions of ResNet such as ResNet50, ResNet34, and ResNet18. The best classification accuracy is marked as **bold**.

Then, the training process for SSDA is conducted in the same manner as the unsupervised domain adaptation (UDA).

Office-Home. As reported in Tab. 12, we compare our student network with previous SSDA works on the **Office-Home** dataset. Remarkably, in terms of mean accuracy, our GraDA (S) surpasses FMLM Basak & Yin (2024) by 19.4% in the 1-shot setting and EFTL He et al. (2024) by 16.1% in the 3-shot setting. Furthermore, our method is not affected by the addition of labeled target samples, with a gain of only 0.6% from the 1-shot to the 3-shot setting.

Office-31. We evaluate our method using the lightweight model, AlexNet Krizhevsky et al. (2012), on **Office-31** under the SSDA setting, as shown in Tab. 13. In the 1-shot and 3-shot settings, our GraDA (S) achieves the new state-of-the-art method with a mean accuracy of 90.8% and 91.7%, respectively.

G Discussion

This section further explores the variety of student networks in GraDA and the pivotal role of CA in teacher network design. We also take a closer look at its impact on student performance through the pseudo-label generation process.

G.1 Robustness with various Student Networks

We investigate the effectiveness of gradient-based knowledge distillation across various student networks. Figures 5 and 6 illustrate results of different versions of the student networks implemented with ResNet50, ResNet34, and ResNet18 for **Office-Home** and ResNet101, ResNet50, and ResNet18 for **VisDA2017**, respectively. Additionally, Tabs. 10 and 11 provide classification accuracy results of various student networks employing ResNet50, ResNet34, and ResNet18 on **Office-31** and **ImageCLEF-DA**. The results presented in these figures and tables demonstrate robustness across various student networks, where smaller networks, such as ResNet18, with relatively fewer parameters, can achieve competitive results compared to larger networks like ResNet50, as shown in Fig. 5, Tabs. 10 and 11, or ResNet101, as illustrated in Fig. 6. For small datasets such as **Office-31** and **ImageCLEF-DA**, the student network based on ResNet18 achieves performance comparable to those based on ResNet50, with only a minimal gap of 0.2%. For moderate and more challenging datasets, such as **Office-Home** and **VisDA2017**, the student network using ResNet18 also demonstrates strong flexibility, closely aligning with the classification results of larger student networks based on ResNet50 or ResNet101.

G.2 Ability of the Teacher Network

Selecting a strong teacher is the most important aspect of knowledge distillation (KD), with various perspectives and definitions. Traditional KD methods often assume that a strong teacher is a large model size. However, (Beyer et al., 2022) argue that a strong teacher is one that is patiently trained

Net	Method	Ar→Cl	Ar→Pr	Ar→Rw	Cl→Ar	Cl→Pr	Cl→Rw	Pr→Ar	Pr→Cl	Pr→Rw	Rw→Ar	Rw→Cl	Rw→Pr	Mean
1-shot														
ResNet34	DECOTA (ICCV'21)	42.1	68.5	72.6	60.3	70.4	70.7	60.0	48.8	76.9	71.3	56.0	79.4	64.8
	APE (ECCV'20)	53.9	76.1	75.2	63.6	69.8	72.3	63.6	58.3	78.6	72.5	60.7	81.6	68.9
	MME (ICCV'19)	59.6	75.5	77.8	65.7	74.5	74.8	64.7	57.4	79.2	71.2	61.9	82.8	70.4
	CLDA (NIPS'21)	56.3	76.1	79.3	66.3	73.9	76.3	66.2	55.9	81.0	72.6	60.2	83.2	70.6
	CDAC (CVPR'21)	61.2	75.9	78.5	64.5	75.1	75.3	64.6	59.3	80.0	72.7	61.9	83.1	71.0
	SPA (NIPS'23)	62.3	76.7	79.0	66.6	77.3	76.4	65.7	59.1	80.7	71.4	65.2	84.1	72.0
	SLA (CVPR'23)	63.0	78.0	79.2	66.9	77.6	77.0	67.3	61.8	80.5	72.7	66.1	84.6	72.9
	MCL (IJCAI'22)	64.4	79.5	81.2	68.5	79.3	78.4	68.0	61.1	81.3	73.8	67.0	85.5	74.0
	EFTL (AAAI'24)	65.7	80.5	80.8	65.6	79.6	77.5	68.7	63.3	82.6	74.3	66.6	87.2	74.4
	ProML (IJCAI'23)	64.5	79.7	81.7	69.1	80.5	79.0	69.3	61.4	81.9	73.7	67.5	86.1	74.6
	FMLM (ECCV'24)	64.1	80.1	81.1	70.6	79.5	79.1	67.9	62.5	80.9	75.2	69.1	87.9	74.8
	🎓 GraDA (S)	**89.9**	**95.5**	**95.8**	**93.5**	**96.3**	**96.9**	**93.7**	**89.1**	**96.9**	**94.5**	**91.2**	**96.9**	**94.2**
ViT-B	🎓 GraDA (T)	90.4	95.6	96.0	93.8	96.4	97.1	93.8	89.6	97.1	94.6	91.5	97.0	94.4
3-shot														
ResNet34	MME (ICCV'19)	63.6	79.0	79.7	67.2	79.3	76.6	65.5	64.6	80.1	71.3	64.6	85.5	73.1
	APE (ECCV'20)	63.9	81.1	80.2	66.6	79.9	76.8	66.1	65.2	82.0	73.4	66.4	86.2	74.0
	CDAC (CVPR'21)	65.9	80.3	80.6	67.4	81.4	80.2	67.5	67.0	81.9	72.2	67.8	85.6	74.2
	SPA (NIPS'23)	63.1	81.0	80.2	68.5	81.7	77.5	69.5	65.2	82.0	73.9	67.2	87.0	74.7
	CLDA (NIPS'21)	63.4	81.4	81.3	70.5	80.9	80.3	72.4	63.9	82.2	76.7	66.0	87.6	75.5
	DECOTA (ICCV'21)	64.0	81.8	80.5	68.0	83.2	79.0	69.9	68.0	82.1	74.0	70.4	87.7	75.7
	SLA (CVPR'23)	67.3	82.6	81.4	69.2	82.1	80.1	70.1	69.3	82.5	73.9	70.1	87.1	76.3
	MCL (IJCAI'22)	67.5	83.9	82.4	71.4	84.3	81.6	69.9	68.0	83.0	75.3	70.1	88.1	77.1
	ProML (IJCAI'23)	67.8	83.9	82.2	72.1	84.1	82.3	72.5	68.9	83.8	75.8	71.0	88.6	77.8
	FMLM (ECCV'24)	68.8	84.7	84.2	70.6	83.7	82.4	70.5	70.9	84.3	75.7	71.1	88.5	77.9
	EFTL (AAAI'24)	70.3	84.8	83.8	70.6	84.6	81.5	72.6	70.9	85.4	77.5	72.8	89.3	78.7
	🎓 GraDA (S)	**91.0**	**96.1**	**97.3**	**93.8**	**96.3**	**97.5**	**94.1**	**90.7**	**97.1**	**94.5**	**92.6**	**97.0**	**94.8**
ViT-B	🎓 GraDA (T)	91.7	96.1	97.4	94.1	96.5	97.8	94.3	91.0	97.3	94.7	93.1	97.1	95.1

Table 12: Accuracy (%) on **Office-Home** under the SSDA setting. The best classification accuracy is marked as **bold**.

Net	Method	W→A		D→A		Mean	
		1-shot	3-shot	1-shot	3-shot	1-shot	3-shot
AlexNet	MME (ICCV'19)	57.2	67.3	55.8	67.8	56.5	67.6
	BiAT (IJCAI'20)	57.9	68.2	54.6	68.5	56.3	68.4
	CDAC (CVPR'21)	63.4	70.1	62.8	70.0	63.1	70.0
	CLDA (NIPS'21)	64.6	70.5	62.7	72.5	63.6	71.5
	ECB (CVPR'24)	77.9	85.2	76.3	84.0	77.1	84.6
	🎓 GraDA (S)	**91.1**	**92.1**	**90.4**	**91.3**	**90.8**	**91.7**
ViT-B	🎓 GraDA (T)	91.9	92.8	91.2	92.4	91.6	92.6

Table 13: Accuracy (%) on **Office-31** under the SSDA setting. The best classification accuracy is marked as **bold**.

over an extended period, producing consistent and reliable outputs. (Martin et al., 2023) propose that a strong teacher dynamically adjusts the amount of knowledge transfer based on the feature gap between the teacher and student models. Similarly, (Sengupta et al., 2024) define a strong teacher as one that can both collaborate with and compete against the student network during the distillation process. However, these approaches typically employ a combination of a feature extractor and an MLP classifier. This setup focuses on *processing individual inputs without considering their neighboring information*. Consequently, the previous teacher networks had limited ability to construct and generalize extracted knowledge effectively.

This section provides further insights into the capabilities of our teacher network. As discussed in the *main manuscript*, the CA module plays a pivotal role in the success of the teacher network's architecture. It effectively explores intra-class relations within each domain, thereby enriching category representations. Additionally, it facilitates class-aware feature alignment across domains, addressing the domain shift issue. To illustrate the superior effectiveness of the CA module, we present additional visualizations of the similarity matrix $\tilde{S}$ on **Office-Home** under the UDA setting and on **DomainNet** under the 3-shot SSDA setting. We use the visualization results from the *left-side figures* in Tabs. 16 and 17 to analyze **the insight operation of our teacher network during training**, including:

Teacher-Student Pair	#Params (M)	Ar→Cl	Ar→Pr	Ar→Rw	Cl→Ar	Cl→Pr	Cl→Rw	Pr→Ar	Pr→Cl	Pr→Rw	Rw→Ar	Rw→Cl	Rw→Pr	Mean
ViT-B+CA (**T**)	89.7	89.3	94.8	97.2	94.1	93.8	96.2	92.8	89.1	97.4	95.1	91.5	97.7	94.0
ResNet50+MLP (**S**)	24.6	88.6	94.8	97.0	93.9	93.7	96.0	92.7	88.3	97.2	95.0	90.9	97.6	93.8
ViT-tiny+MLP (**S**)	5.7	87.0	93.1	96.2	93.6	93.8	95.7	92.1	87.0	96.0	94.6	88.2	96.9	92.9
ResNet50+CA (**T**)	30.3	78.3	87.6	95.3	81.5	83.9	89.7	84.8	75.9	93.8	92.5	82.8	93.0	86.6
ResNet50+MLP (**S**)	24.6	77.8	87.3	95.1	81.4	83.8	89.5	84.6	75.5	93.5	92.3	82.5	92.9	86.4
ViT-tiny+CA (**T**)	8.1	68.7	84.6	89.9	82.0	81.4	84.5	83.7	69.6	93.0	87.5	75.6	91.9	82.7
ViT-tiny+MLP (**S**)	5.7	68.3	82.9	89.0	81.8	80.5	82.9	83.6	69.1	92.8	87.3	75.1	90.8	82.0
HVCLIP (ResNet50)	≈101.5	62.0	85.8	86.2	77.8	84.3	86.8	80.7	66.5	87.8	80.3	64.9	90.4	79.5

Table 14: Comparison of teacher-student pairs on **Office-Home** under the UDA setting (*Full version*).

- **Enhancing the generalization by enriching intra-class relations.** We process a batch of $B = 16$ images through the teacher network, covering two classes, as an example. For each class, there are *four samples from the source domain* and another *four samples from the target domain*. For easier visualization, source samples are marked in green, while target samples are marked in pink. The CA module works effectively to show high similarity scores for same-category samples within the source domain indicated by dashed green. This is intuitive, as the source ground truth information supports these results. For target samples, the CA module relies on the quality of generated pseudo labels. Despite this, it still assigns high similarity scores to samples belonging to the same class, as marked by dashed pink boxes.

- **Handling the domain shift via class-aware feature alignment.** To demonstrate the effectiveness of the CA module in the teacher network for handling the domain shift issue between the source and target domains, we present the similarity scores of cross-domain samples highlighted by dashed yellow boxes. The CA module successfully identifies samples belonging to the same class but from different domains by assigning high similarity scores. In contrast, it assigns low similarity scores to samples from distinct classes, ensuring robust class-aware feature alignment.

These observations strongly emphasize the capability of the CA module in teacher network design. Furthermore, unlike previous teacher networks that make predictions directly from features extracted by the feature extractor, our teacher network bases its predictions on aggregated features.

Effectiveness of the teacher network in the testing phase. We use the visualization results from the *right-side figures* in Tabs. 16 and 17 to evaluate the effectiveness of the teacher network during testing. As illustrated in these figures, the CA module effectively identifies target samples within the same category by assigning high similarity scores, while providing low similarity scores to samples from distinct classes. This observation highlights the teacher network's capability to exploit intra-class relations within the target data, grouping samples of the same category while ensuring that samples from different classes remain distinguishable.

G.3 Roles of CA Module in Pseudo-Labeling

To demonstrate the effectiveness of our CA module in the pseudo-labeling process, we compare the quantity and quality of pseudo labels generated by ViT-B+MLP (**Setting 1**) and ViT-B+CA (**Setting 2**) as teacher networks on **VisDA2017**. As shown in Fig. 7, the dashed lines indicate the number of ground-truth labels for each class, while the colored bars represent the pseudo-label counts. These two settings follow the same training manner combining *supervised*, *self-enhanced*, and *cross-class confusion* strategies.

In **Setting 1**, we employ MLP as the classifier, which is unable to capture relationships among neighboring samples. As illustrated in Fig. 7a, the ViT-B+MLP network assigns a higher number of pseudo labels than ground-truth labels to classes such as "*bicycle*", "*bus*", "*skate*", and "*truck*". Obviously, those excessive pseudo labels are incorrect, indicating that ViT-B+MLP does not ensure the quality of its generated pseudo labels, which misguide the student network. Furthermore, as it focuses only on individual representations, the MLP classifier also demonstrates its weakness in differentiating between highly similar classes, such as "*bus*", "*car*", "*train*", and "*truck*".

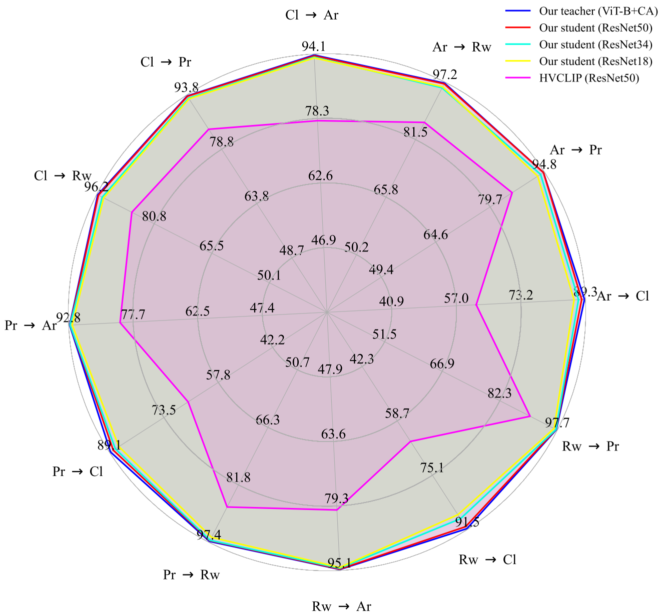

Figure 5: Performance of the teacher network and its three students on the **Office-Home** dataset under the UDA setting. The black numbers on the radar chart indicate the distance values from the center to the corresponding intersections of the concentric circles. The classification results show that our method performs effectively across various student network configurations. It remains unaffected by the capability gap between teacher and student networks and significantly surpasses the second-best approach, HVCLIP (Vesdapunt et al., 2024), even with a student network using fewer parameters.

Teacher-Student Pair		#Param. (**M**)	Ar→Cl	Cl→Pr	Pr→Rw	Rw→Ar	Mean
T	ViT-B+CA	89.7	89.3	93.8	97.4	95.1	93.9
S	ResNet50+MLP	24.6	88.6	93.7	97.2	95.0	93.6
	ResNet34+MLP	21.6	87.8	93.2	97.1	94.8	93.2
	ResNet18+MLP	11.5	86.7	93.1	96.3	94.6	92.7

Table 15: Accuracy of different student network (**S**) paired with the fixed teacher network (**T**) on **Office-Home** under the UDA setting.

In contrast, in **Setting 2**, the proposed CA module enriches intra-class relationships by aggregating representations of samples within the same category. This enables the ViT-B+CA network to enhance the robustness of representations within each class. As a result, the ViT-B+CA network demonstrates stronger discriminability between different classes compared to the ViT-B+MLP network. This can be observed clearly in the *car* class, where the quantity and quality of pseudo labels generated by **Setting 2** are significantly higher than those of **Setting 1**, as shown in Figs. 7a and 7b. By doing so, the ViT-B+CA teacher network can provide more reliable information to train the student network, resulting in a substantial increase in the overall results of the student network.

G.4 Effectiveness of Gradient-Based KD

We first provide the method to visualize the gradient trajectories of teacher and student networks, learnable parameters and their corresponding loss values from all episodes are used: $\{\theta_T^e, l_T^e\}_{e=1}^E$ and $\{\theta_S^e, l_S^e\}_{e=1}^E$, where $\theta_T = \{\theta_{vit}, \theta_{sim}, \theta_{agg}\}$, and $\theta_S = \{\theta_{cnn}, \theta_{mlp}\}$. Here, l_T^e and l_S^e are per-epoch loss values of the teacher and student networks, respectively. The parameters $\{\theta_T^e\}_{e=1}^E$ and

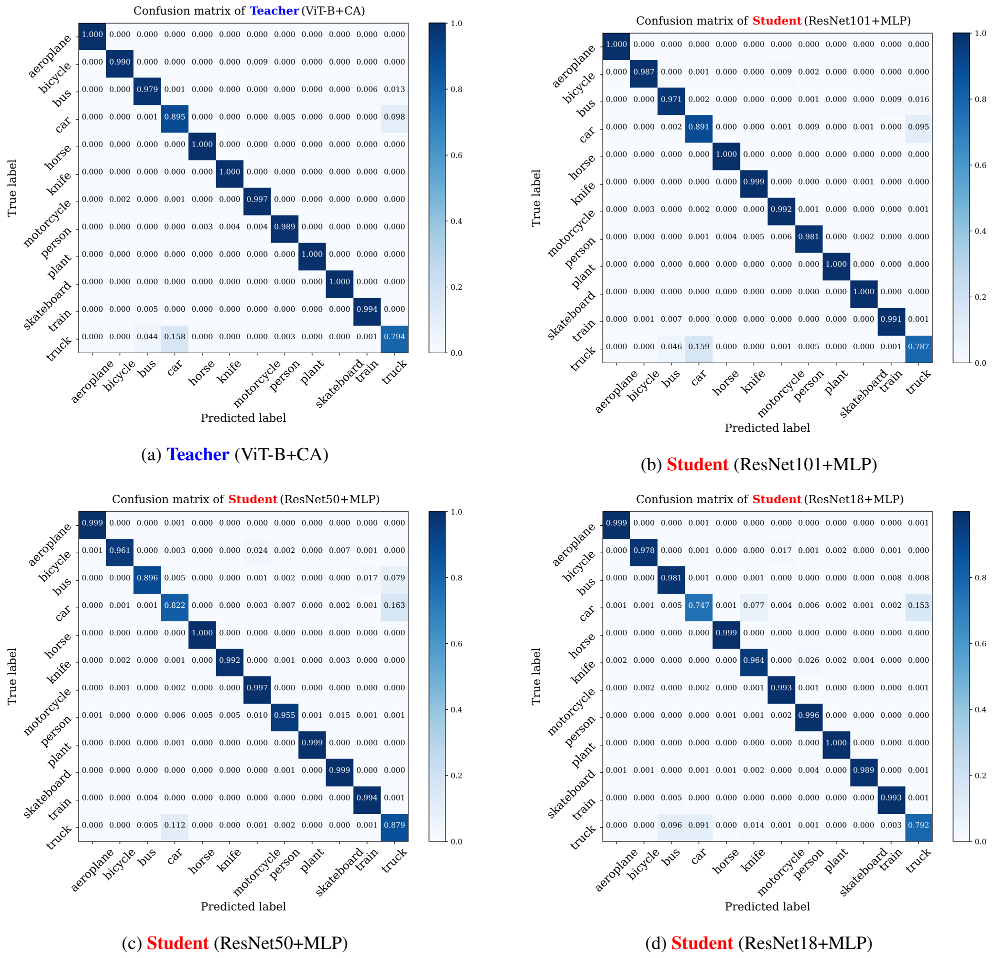

(a) Teacher (ViT-B+CA)

(b) Student (ResNet101+MLP)

(c) Student (ResNet50+MLP)

(d) Student (ResNet18+MLP)

Figure 6: Confusion matrix of (a) the teacher network, and (b), (c), (d) representing various student networks, specifically ResNet101, ResNet50, and ResNet18, respectively. These networks are evaluated across 12 classes on **VisDA2017** under the UDA setting.

$\{\theta_S^e\}_{e=1}^E$ are projected into 2D space using UMAP McInnes et al. (2018), yielding $\tilde{\boldsymbol{\theta}}_T = \{\tilde{\theta}_T^e\}_{e=1}^E$ and $\tilde{\boldsymbol{\theta}}_S = \{\tilde{\theta}_S^e\}_{e=1}^E$, where $\tilde{\theta}_T^e, \tilde{\theta}_S^e \in \mathbb{R}^2$. The student projections $\tilde{\boldsymbol{\theta}}_S$ are scaled to match the value range of $\tilde{\boldsymbol{\theta}}_T$. We then sum up the loss values of the two networks per epoch to obtain a set of combined loss values, $L = \{l_T^e + l_S^e\}_{e=1}^E$. The variables $\tilde{\boldsymbol{\theta}}_S$, $\tilde{\boldsymbol{\theta}}_T$, and L are used to estimate the loss landscape using cubic interpolation. Finally, $\tilde{\boldsymbol{\theta}}_S$, $\tilde{\boldsymbol{\theta}}_T$, and the loss landscape are plotted to illustrate the gradient trajectories of the two networks, showing the direction of their convergency in the respective minima.

We provide additional results of the gradient trajectory visualization with various student networks such as ResNet50, ResNet34, and ResNet18 for the Ar→Cl, Ar→Pr, Pr→Ar, and Rw→Cl tasks from the **Office-Home** dataset in Tab. 18. These results demonstrate that the teacher network effectively guides the student, regardless of various student network architectures, within our GraDA framework, further validating its reliability for DA tasks.

G.5 Fairness of the Teacher Network (*Extended Version*).

This study presents an enhanced approach to fairness evaluation, extending comparisons across multiple teacher networks. Experimental outcomes full 12 domain adaptation tasks, utilizing the **Office-Home** dataset, are detailed in Table 14. Notably, networks employing the robust ViT-B+CA teacher model (denoted as (**S**)) demonstrate superior performance. Furthermore, the proposed CA module proves effective when integrated with either the ResNet50 architecture or the more compact ViT-Tiny model. The student network (**S**) supported by the CA-based teacher network (**T**) consistently surpasses the second-best method, HVCLIP, highlighting that its performance improvements derive primarily from the CA module and the efficacy of pseudo-labeling, rather than solely from the backbone architecture.

G.6 Can the Teacher Adapt to Various Students?

To explore this concern, we construct diverse student networks, including ResNet50+MLP, ResNet34+MLP, and ResNet18+MLP, while fixing ViT-B+CA as the teacher network. As listed in Table 15, the experimental results across 4 DA tasks on **Office-Home** under the UDA setting demonstrate that GraDA is effective regardless of the student network used. Surprisingly, despite having considerably fewer parameters than ResNet34 and ResNet50, the student network based on ResNet18 achieves competitive performance, with small performance gaps of 0.5% and 0.9%, respectively.

H Visualization Analysis

In this section, t-SNE Van der Maaten & Hinton (2008) visualizations are provided to show embedding improvements across training strategies, while Grad-CAM Selvaraju et al. (2017) is used to demonstrate the enhanced visual performance of the student network in GraDA.

H.1 t-SNE Visualization

We use t-SNE Van der Maaten & Hinton (2008) to further evaluate the effectiveness of the proposed gradient-based knowledge distillation for domain adaptation via visualizing domain alignment and target feature distributions. Figure 8 presents the visualization results of the Rw→Cl task on **Office-Home** under the UDA setting, while Fig. 9 illustrates results of the rel→pnt task on **DomainNet** under the SSDA setting (3-shot). We first show results of the vanilla student trained using *supervised*, *self-enhanced*, and *cross-class confusion* losses without guidance from the teacher network, as specified in setting **S3** of the *main manuscript*. Then, we investigate the impact of the teacher network on the feature space of the student network by progressively adding *supervised* (**Teacher+S4**), *self-enhanced* (**Teacher+S5**), and *cross-class confusion* (**Teacher+S6**) settings.

The vanilla student (**S3**) struggles to provide robust representations due to the sensitivity of CNN to domain shift and its limited ability to capture relationships among neighboring samples. As shown in Figs. 8a and 9a, the target features are highly misalignment compared to those guided by the teacher network under the **Teacher+S4** setting (Figs. 8b and 9b) thanks to ability in enriching intra-class relations. In cases **Teacher+S5**, the teacher network leverages pseudo labels generated from unlabeled target data to enhance intra-class information on the target domain and mitigating domain shifts through *class-aware feature alignment*. As shown in Figs. 8c and 9c, the teacher network effectively guides the student network using these pseudo labels, enabling the student to align source and target features. Additionally, the discriminative ability among the different classes of the student network is also improved, as illustrated in Figs. 8g and 9g. Finally, we implement the cross-class confusion loss in the **Teacher+S6** setting to reduce ambiguous prediction among classes, resulting in a slight improvement, as shown in Figs. 8d and 8h for **Office-Home**, and Figs. 9d and 9h for **DomainNet**.

H.2 Grad-CAM Visualization

We visualize attention maps to examine our gradient-guided ability of the teacher network for the student network by using Grad-CAM Selvaraju et al. (2017). To clearly demonstrate the improvements of our student network, GraDA (S), over the vanilla student network (without any guidance), we present samples that are misclassified by the vanilla student but correctly classified by GraDA (S) under the UDA and SSDA settings on the **Office-Home** and **DomainNet** datasets.

Office-Home. For the **Office-Home** dataset under UDA, we present attention results for four tasks: Ar→Cl, Cl→Pr, Pr→Rw, and Rw→Ar. In both the vanilla student network and GraDA (S), ResNet50 is utilized as the feature extractor. As shown in Tab. 19, without any guidance, the vanilla student network struggles to capture object regions in several classes, such as "*alarm clock*", "*keyboard*", "*spoon*", "*bucket*", *chair*", "*couch*", "*flipflops*", "*flowers*", and "*shelf*". Meanwhile, GraDA (**S**) is shown to focus more precise regions, shifting focus from irrelevant to relevant elements, such as from a cable to a "*keyboard*" or a broom to a "*bucket*". Upon closer examination, it is clear that GraDA (**S**) closely emulates the behavior of GraDA (**T**), which itself demonstrates strong performance. For example, in the case of the class "*bed*", the vanilla student network fails to capture the entire bed and instead focuses only on the footboard, leading to the wrong prediction. However, our teacher network successfully captures the full object, enabling our student network, GraDA (**S**), to learn and mimic this behavior. Similar observations are evident for "*batteries*", "*post-it notes*", "*toothbrush*", and "*toys*".

DomainNet. For the **DomainNet** dataset under SSDA, we extract the attention results for four tasks: rel→clp, clp→skt, skt→pnt, and pnt→rel, which are shown in Tab. 20. ResNet34 is utilized as a feature extractor for the student network. Overall, we observe that the teacher network GraDA (**T**) accurately captures the salient regions that strongly represent the class label of the image. For samples containing a single instance, such as "*crab*," the teacher network accurately focuses on the crab in the center, effectively guiding the student to mimic this behavior. In contrast, the vanilla student focuses only on the frame, which provides no key information and ultimately leads to misclassification. Same observations are evident for "*cell phone*", "*spider*", "*alarm clock*", "*bus*", and "*submarine*". In the case of multiple instances appearing in an image, two scenarios can be identified: 1) instances with similar characteristics and 2) salient instances that are mixed with miscellaneous or less relevant instances. In the first scenario, for example, an ant appears with a book in the "*ant*" class, and a cello appears with a panda in the "*cello*" class. This can lead to confusion. Interestingly, the student network guided by GraDA (**T**) is shown to correctly focus on the salient instances, precisely detecting the ant's head in the "*ant*" class and effectively separating the cello from the panda in the "*cello*" class. In contrast, the vanilla student fails to do so, focusing on completely irrelevant instances in all cases. Similar observations are evident for the "*cactus*", "*cell phone*", and "*banana*" classes. In the second scenario, where multiple instances with similar characteristics appear, our student network successfully covers all of them. For example, GraDA (**S**) captures all dolphins and all rabbits in the "*dolphin*" and "*rabbit*" classes, respectively, whereas the vanilla student focuses on only one instance. Similar observations are made for the "*whale*" and "*sheep*" classes.

Intra-class relations and Class-aware alignment (during training)	**Intra-class relations on target domain only (during testing)**
Art→Clipart	
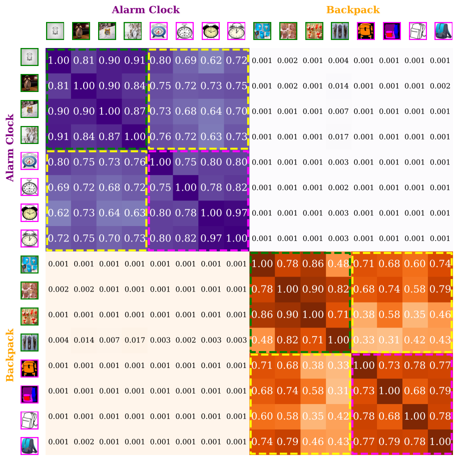	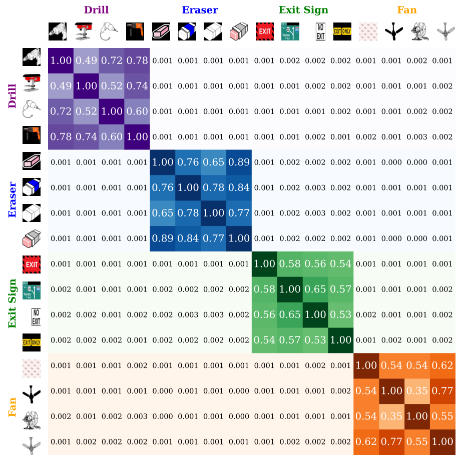

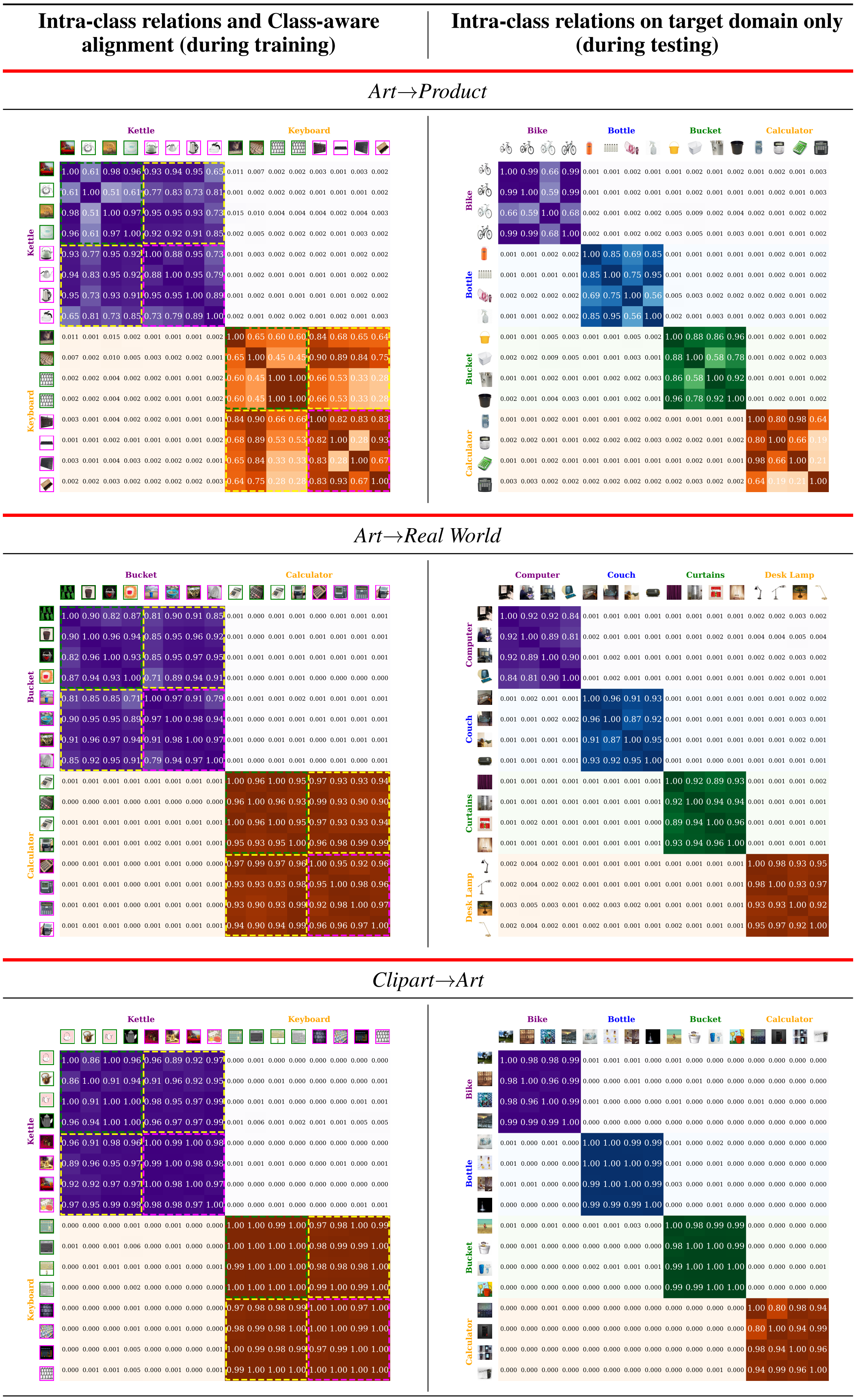
Intra-class relations and Class-aware alignment (during training)
Intra-class relations on target domain only (during testing)
Art→Product
Kettle
Keyboard
Bike
Bottle
Bucket
Calculator
Art→Real World
Bucket
Calculator
Computer
Couch
Curtains
Desk Lamp
Clipart→Art
Kettle
Keyboard
Bike
Bottle
Bucket
Calculator

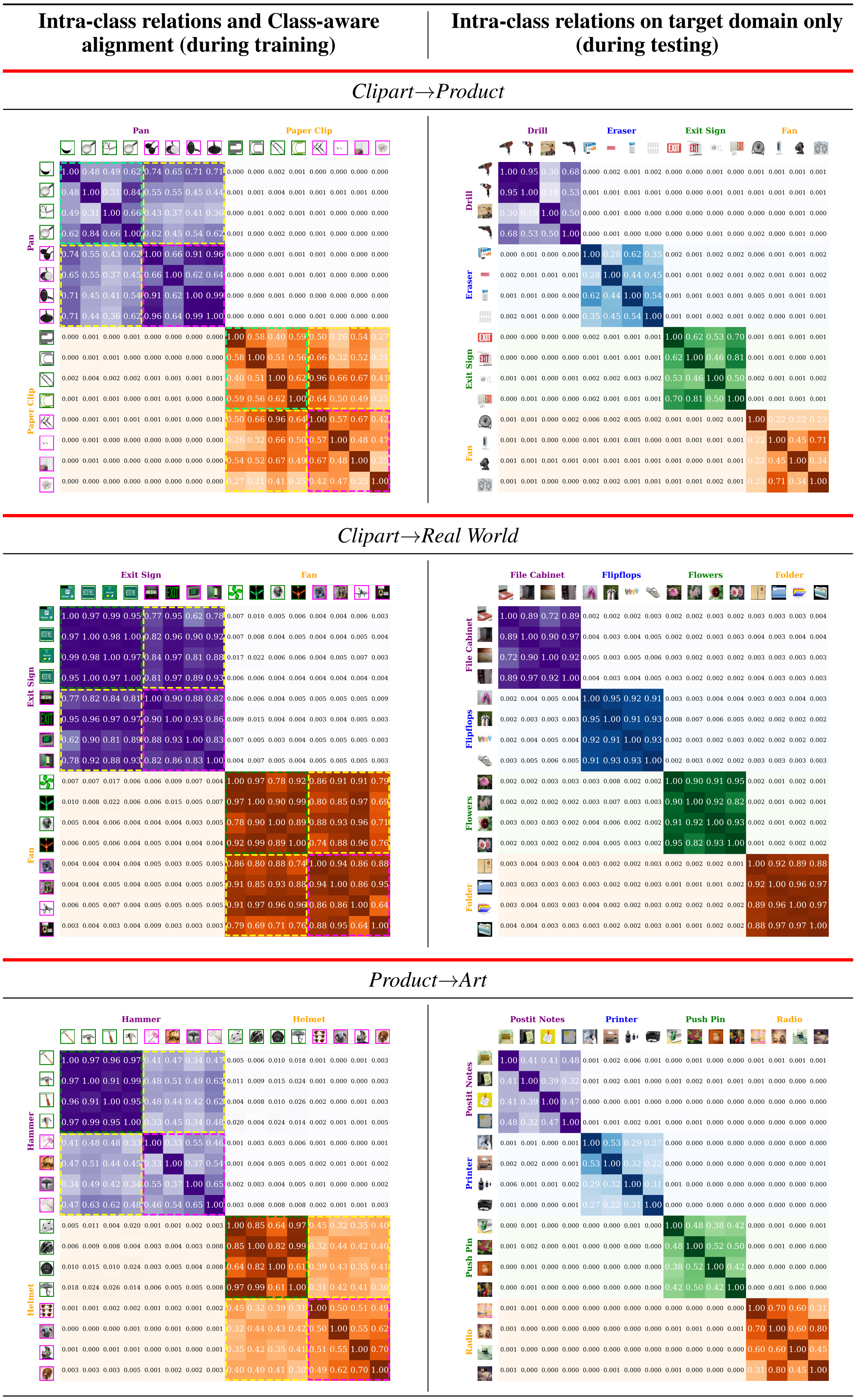
Intra-class relations and Class-aware alignment (during training)
Intra-class relations on target domain only (during testing)
Clipart→Product
Pan
Paper Clip
Drill
Eraser
Exit Sign
Fan
Clipart→Real World
Exit Sign
Fan
File Cabinet
Flipflops
Flowers
Folder
Product→Art
Hammer
Helmet
Postit Notes
Printer
Push Pin
Radio

Intra-class relations and Class-aware alignment (during training)

Intra-class relations on target domain only (during testing)

Product→Clipart

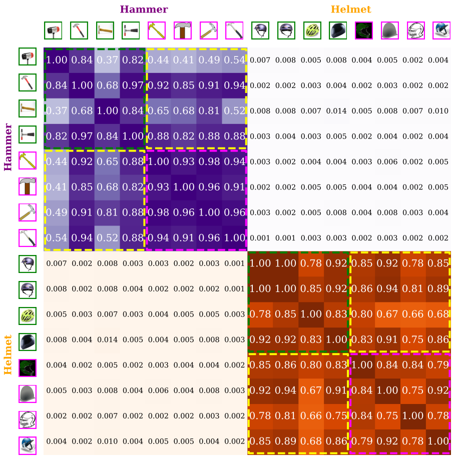

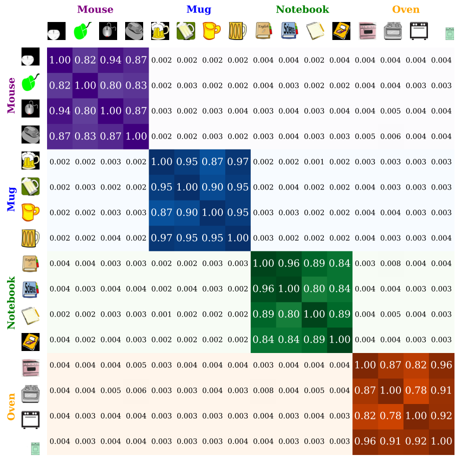

Product→Real World

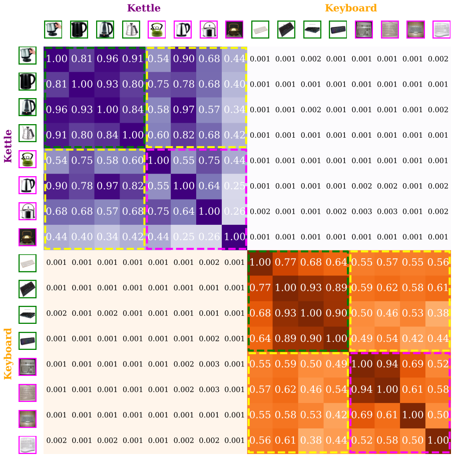

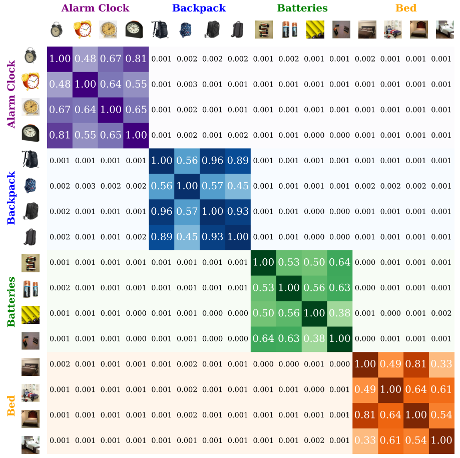

Real World→Art

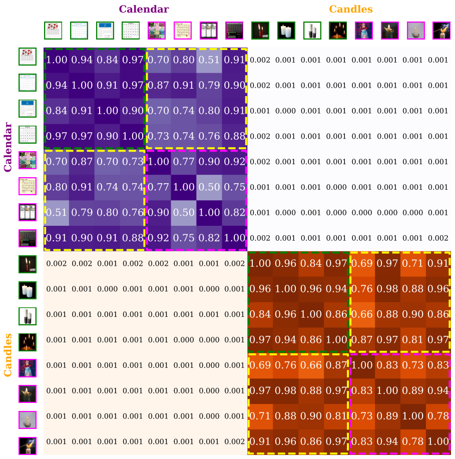

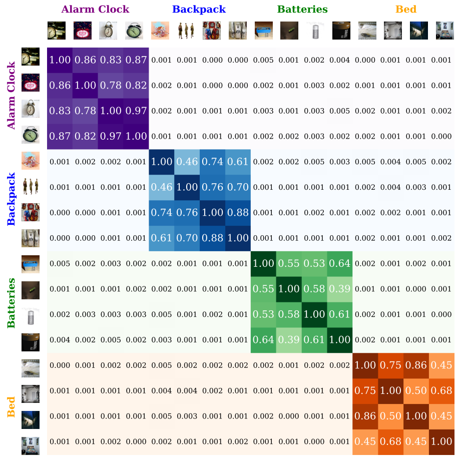

Intra-class relations and Class-aware alignment (during training)	**Intra-class relations on target domain only (during testing)**

Real World→Clipart

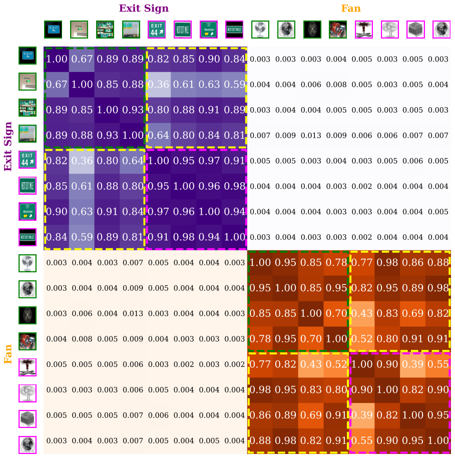

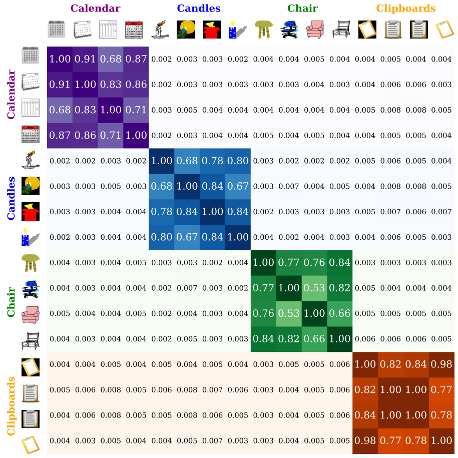

Real World→Product

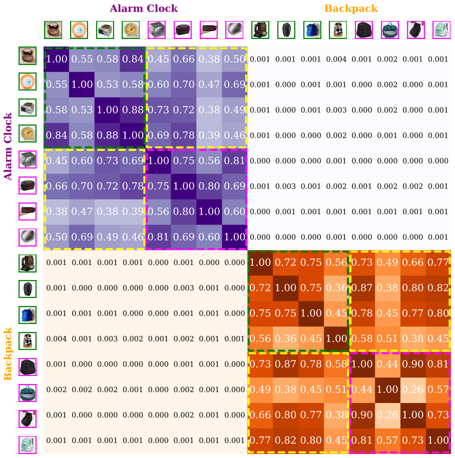

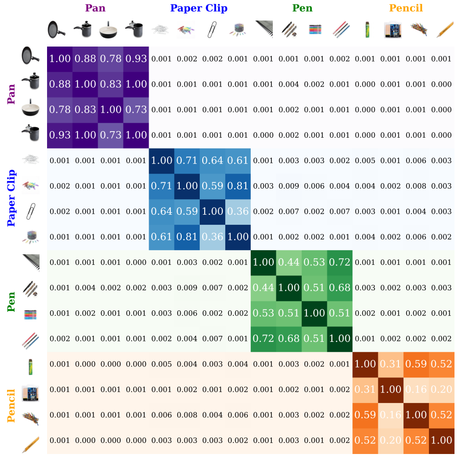

Table 16: Similarity matrix $\tilde{S}$ of the 12 UDA tasks on the **Office-Home** dataset. Dashed green and pink boxes are marked for the relationships of samples within the source and target domains, respectively. The dashed yellow boxes outline the relationships of cross-domain samples. Higher values reflect greater similarity scores.

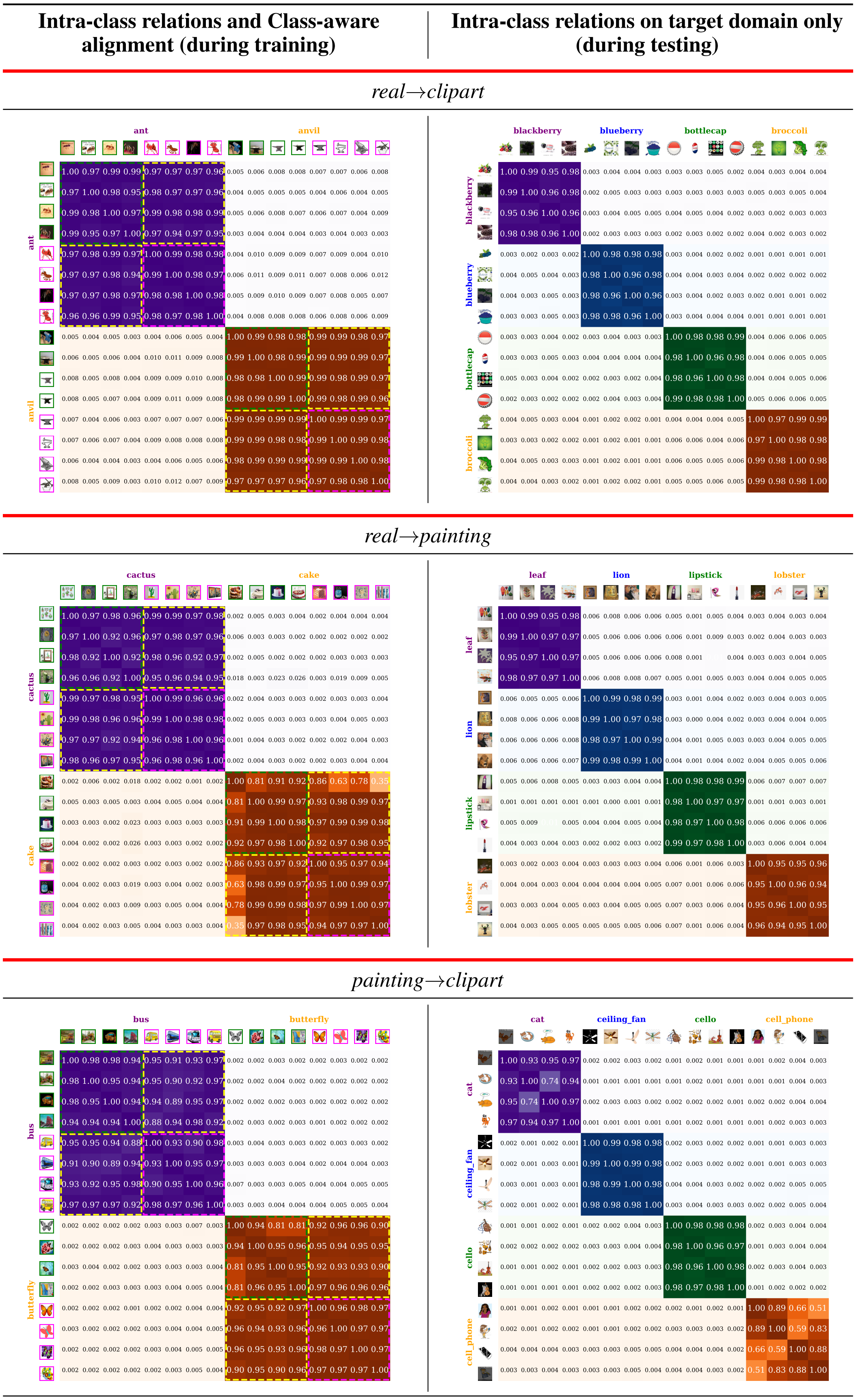

Intra-class relations and Class-aware alignment (during training)

Intra-class relations on target domain only (during testing)

real→clipart

real→painting

painting→clipart

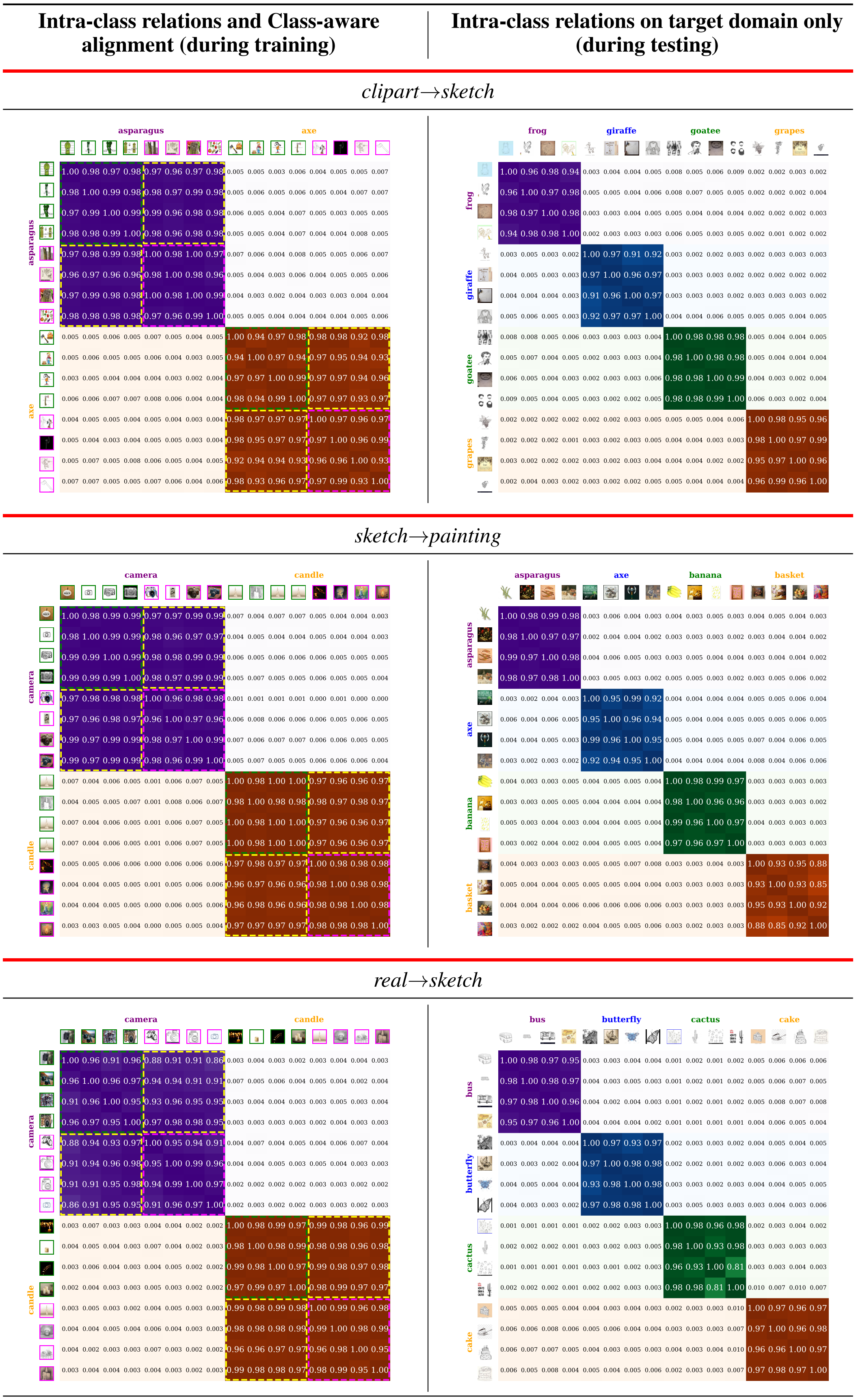
Intra-class relations and Class-aware alignment (during training)
Intra-class relations on target domain only (during testing)
clipart→sketch
asparagus
axe
asparagus 1.00 0.98 0.97 0.98 0.97 0.96 0.97 0.98 0.005 0.005 0.003 0.006 0.004 0.005 0.005 0.007
0.98 1.00 0.99 0.98 0.98 0.97 0.99 0.98 0.005 0.006 0.005 0.006 0.005 0.004 0.007 0.007
0.97 0.99 1.00 0.99 0.99 0.96 0.98 0.98 0.006 0.005 0.004 0.007 0.005 0.003 0.005 0.005
0.98 0.98 0.99 1.00 0.98 0.96 0.98 0.98 0.005 0.005 0.004 0.007 0.004 0.004 0.008 0.005
0.97 0.98 0.99 0.98 1.00 0.98 1.00 0.97 0.007 0.006 0.004 0.008 0.005 0.005 0.006 0.007
0.96 0.97 0.96 0.96 0.98 1.00 0.98 0.96 0.005 0.004 0.003 0.006 0.004 0.005 0.005 0.006
0.97 0.99 0.98 0.98 1.00 0.98 1.00 0.99 0.004 0.003 0.002 0.004 0.003 0.003 0.004 0.004
0.98 0.98 0.98 0.98 0.97 0.96 0.99 1.00 0.005 0.005 0.004 0.004 0.004 0.004 0.005 0.006
axe 0.005 0.005 0.006 0.005 0.007 0.005 0.004 0.005 1.00 0.94 0.97 0.98 0.98 0.98 0.92 0.98
0.005 0.006 0.005 0.005 0.006 0.004 0.003 0.005 0.94 1.00 0.97 0.94 0.97 0.95 0.94 0.93
0.003 0.005 0.004 0.004 0.004 0.003 0.002 0.004 0.97 0.97 1.00 0.99 0.97 0.97 0.94 0.96
0.006 0.006 0.007 0.007 0.008 0.006 0.004 0.004 0.98 0.94 0.99 1.00 0.97 0.97 0.93 0.97
0.004 0.005 0.005 0.004 0.005 0.004 0.003 0.004 0.98 0.97 0.97 0.97 1.00 0.97 0.96 0.97
0.005 0.004 0.003 0.004 0.005 0.005 0.003 0.004 0.98 0.95 0.97 0.97 0.97 1.00 0.96 0.99
0.005 0.007 0.005 0.008 0.006 0.005 0.004 0.005 0.92 0.94 0.94 0.93 0.96 0.96 1.00 0.93
0.007 0.007 0.005 0.005 0.007 0.006 0.004 0.006 0.98 0.93 0.96 0.97 0.97 0.99 0.93 1.00
frog
giraffe
goatee
grapes
frog 1.00 0.96 0.98 0.94 0.003 0.004 0.004 0.005 0.008 0.005 0.006 0.009 0.002 0.002 0.003 0.002
0.96 1.00 0.97 0.98 0.005 0.005 0.004 0.006 0.008 0.007 0.005 0.005 0.002 0.002 0.002 0.004
0.98 0.97 1.00 0.98 0.003 0.003 0.004 0.005 0.005 0.004 0.004 0.004 0.002 0.002 0.002 0.003
0.94 0.98 0.98 1.00 0.002 0.003 0.003 0.003 0.006 0.005 0.003 0.005 0.002 0.001 0.002 0.002
giraffe 0.003 0.005 0.003 0.002 1.00 0.97 0.91 0.92 0.003 0.002 0.002 0.003 0.002 0.003 0.003 0.003
0.004 0.005 0.003 0.003 0.97 1.00 0.96 0.97 0.003 0.003 0.003 0.002 0.002 0.002 0.002 0.002
0.004 0.004 0.004 0.003 0.91 0.96 1.00 0.97 0.003 0.003 0.003 0.002 0.003 0.003 0.003 0.002
0.005 0.006 0.005 0.003 0.92 0.97 0.97 1.00 0.004 0.004 0.006 0.005 0.005 0.005 0.004 0.005
goatee 0.008 0.008 0.005 0.006 0.003 0.003 0.003 0.004 1.00 0.98 0.98 0.98 0.005 0.004 0.004 0.005
0.005 0.007 0.004 0.005 0.002 0.003 0.003 0.004 0.98 1.00 0.98 0.98 0.005 0.004 0.004 0.004
0.006 0.005 0.004 0.003 0.002 0.003 0.003 0.006 0.98 0.98 1.00 0.99 0.004 0.003 0.002 0.004
0.009 0.005 0.004 0.005 0.003 0.002 0.002 0.005 0.98 0.98 0.99 1.00 0.006 0.003 0.002 0.004
grapes 0.002 0.002 0.002 0.002 0.002 0.002 0.003 0.005 0.005 0.005 0.004 0.006 1.00 0.98 0.95 0.96
0.002 0.002 0.002 0.001 0.003 0.002 0.003 0.005 0.004 0.004 0.003 0.003 0.98 1.00 0.97 0.99
0.003 0.002 0.002 0.002 0.003 0.002 0.003 0.004 0.004 0.004 0.002 0.002 0.95 0.97 1.00 0.96
0.002 0.004 0.003 0.002 0.003 0.002 0.002 0.005 0.005 0.004 0.004 0.004 0.96 0.99 0.96 1.00
sketch→painting
camera
candle
camera 1.00 0.98 0.99 0.99 0.97 0.97 0.99 0.99 0.007 0.004 0.007 0.007 0.005 0.004 0.004 0.003
0.98 1.00 0.99 0.99 0.98 0.96 0.97 0.97 0.004 0.005 0.004 0.004 0.005 0.004 0.004 0.003
0.99 0.99 1.00 0.99 0.98 0.98 0.99 0.99 0.006 0.005 0.006 0.006 0.006 0.005 0.005 0.005
0.99 0.99 0.99 1.00 0.98 0.97 0.99 0.99 0.005 0.007 0.005 0.005 0.006 0.005 0.005 0.004
0.97 0.98 0.98 0.98 1.00 0.96 0.98 0.98 0.001 0.001 0.001 0.001 0.000 0.001 0.000 0.000
0.97 0.96 0.98 0.97 0.96 1.00 0.97 0.96 0.006 0.008 0.006 0.006 0.006 0.005 0.006 0.005
0.99 0.97 0.99 0.99 0.98 0.97 1.00 0.99 0.007 0.006 0.007 0.007 0.006 0.006 0.005 0.005
0.99 0.97 0.99 0.99 0.98 0.96 0.99 1.00 0.005 0.007 0.005 0.005 0.006 0.006 0.006 0.004
candle 0.007 0.004 0.006 0.005 0.001 0.006 0.007 0.005 1.00 0.98 1.00 1.00 0.97 0.96 0.96 0.97
0.004 0.005 0.005 0.007 0.001 0.008 0.006 0.007 0.98 1.00 0.98 0.98 0.98 0.97 0.98 0.97
0.007 0.004 0.006 0.005 0.001 0.006 0.007 0.005 1.00 0.98 1.00 1.00 0.97 0.96 0.96 0.97
0.007 0.004 0.006 0.005 0.001 0.006 0.007 0.005 1.00 0.98 1.00 1.00 0.97 0.96 0.96 0.97
0.005 0.005 0.006 0.006 0.000 0.006 0.006 0.006 0.97 0.98 0.97 0.97 1.00 0.98 0.98 0.98
0.004 0.004 0.005 0.005 0.001 0.005 0.006 0.006 0.96 0.97 0.96 0.96 0.98 1.00 0.98 0.98
0.004 0.004 0.005 0.005 0.000 0.006 0.005 0.006 0.96 0.98 0.96 0.96 0.98 0.98 1.00 0.98
0.003 0.003 0.005 0.004 0.000 0.005 0.005 0.004 0.97 0.97 0.97 0.97 0.98 0.98 0.98 1.00
asparagus
axe
banana
basket
asparagus 1.00 0.98 0.99 0.98 0.003 0.006 0.004 0.003 0.004 0.003 0.005 0.003 0.004 0.005 0.004 0.003
0.98 1.00 0.97 0.97 0.002 0.004 0.004 0.002 0.003 0.003 0.003 0.002 0.003 0.004 0.004 0.002
0.99 0.97 1.00 0.98 0.004 0.006 0.005 0.003 0.003 0.005 0.004 0.004 0.003 0.004 0.004 0.002
0.98 0.97 0.98 1.00 0.003 0.005 0.003 0.002 0.005 0.005 0.003 0.002 0.003 0.005 0.006 0.002
axe 0.003 0.002 0.004 0.003 1.00 0.95 0.99 0.92 0.004 0.004 0.004 0.004 0.005 0.005 0.006 0.004
0.006 0.004 0.006 0.005 0.95 1.00 0.96 0.94 0.005 0.004 0.004 0.005 0.005 0.005 0.006 0.005
0.004 0.004 0.005 0.003 0.99 0.96 1.00 0.95 0.005 0.004 0.005 0.005 0.007 0.004 0.006 0.005
0.003 0.002 0.003 0.002 0.92 0.94 0.95 1.00 0.004 0.004 0.004 0.004 0.008 0.004 0.006 0.006
banana 0.004 0.003 0.003 0.005 0.004 0.005 0.005 0.004 1.00 0.98 0.99 0.97 0.003 0.003 0.003 0.003
0.003 0.003 0.005 0.005 0.004 0.004 0.004 0.004 0.98 1.00 0.96 0.96 0.003 0.003 0.003 0.002
0.005 0.003 0.004 0.003 0.004 0.004 0.005 0.004 0.99 0.96 1.00 0.97 0.004 0.003 0.003 0.003
0.003 0.002 0.004 0.002 0.004 0.005 0.005 0.004 0.97 0.96 0.97 1.00 0.003 0.003 0.003 0.003
basket 0.004 0.003 0.003 0.003 0.005 0.005 0.007 0.008 0.003 0.003 0.004 0.003 1.00 0.93 0.95 0.88
0.005 0.004 0.004 0.005 0.005 0.005 0.004 0.004 0.003 0.003 0.003 0.003 0.93 1.00 0.93 0.85
0.004 0.004 0.004 0.006 0.006 0.006 0.006 0.006 0.003 0.003 0.003 0.003 0.95 0.93 1.00 0.92
0.003 0.002 0.002 0.002 0.004 0.005 0.005 0.006 0.003 0.002 0.003 0.003 0.88 0.85 0.92 1.00
real→sketch
camera
candle
camera 1.00 0.96 0.91 0.96 0.88 0.91 0.91 0.86 0.003 0.004 0.003 0.002 0.003 0.004 0.004 0.003
0.96 1.00 0.96 0.97 0.94 0.94 0.91 0.91 0.007 0.005 0.006 0.004 0.005 0.004 0.002 0.004
0.91 0.96 1.00 0.95 0.93 0.96 0.95 0.95 0.003 0.004 0.004 0.003 0.003 0.005 0.003 0.004
0.96 0.97 0.95 1.00 0.97 0.98 0.98 0.95 0.003 0.003 0.003 0.003 0.002 0.004 0.003 0.003
0.88 0.94 0.93 0.97 1.00 0.95 0.94 0.91 0.004 0.007 0.004 0.005 0.004 0.006 0.007 0.004
0.91 0.94 0.96 0.98 0.95 1.00 0.99 0.96 0.004 0.004 0.005 0.003 0.005 0.004 0.003 0.003
0.91 0.91 0.95 0.98 0.94 0.99 1.00 0.97 0.002 0.002 0.002 0.002 0.003 0.003 0.002 0.002
0.86 0.91 0.95 0.95 0.91 0.96 0.97 1.00 0.002 0.003 0.002 0.002 0.003 0.003 0.002 0.003
candle 0.003 0.007 0.003 0.003 0.004 0.004 0.002 0.002 1.00 0.98 0.99 0.97 0.99 0.98 0.96 0.99
0.004 0.005 0.004 0.003 0.007 0.004 0.002 0.003 0.98 1.00 0.98 0.99 0.98 0.98 0.96 0.98
0.003 0.006 0.004 0.003 0.004 0.005 0.002 0.002 0.99 0.98 1.00 0.97 0.99 0.98 0.97 0.98
0.002 0.004 0.003 0.003 0.005 0.003 0.002 0.002 0.97 0.99 0.97 1.00 0.98 0.99 0.97 0.97
0.003 0.005 0.003 0.002 0.004 0.005 0.003 0.003 0.99 0.98 0.99 0.98 1.00 0.99 0.96 0.98
0.004 0.004 0.005 0.004 0.006 0.004 0.003 0.003 0.98 0.98 0.98 0.99 0.99 1.00 0.98 0.99
0.004 0.002 0.003 0.003 0.007 0.003 0.002 0.002 0.96 0.96 0.97 0.97 0.96 0.98 1.00 0.95
0.003 0.004 0.004 0.003 0.004 0.003 0.002 0.003 0.99 0.98 0.98 0.97 0.98 0.99 0.95 1.00
bus
butterfly
cactus
cake
bus 1.00 0.98 0.97 0.95 0.003 0.003 0.004 0.004 0.001 0.002 0.001 0.002 0.005 0.006 0.006 0.006
0.98 1.00 0.98 0.97 0.004 0.003 0.005 0.003 0.001 0.002 0.001 0.002 0.005 0.006 0.007 0.005
0.97 0.98 1.00 0.96 0.004 0.002 0.004 0.003 0.001 0.002 0.001 0.002 0.005 0.008 0.007 0.008
0.95 0.97 0.96 1.00 0.004 0.004 0.004 0.002 0.001 0.001 0.001 0.001 0.004 0.006 0.005 0.004
butterfly 0.003 0.004 0.004 0.004 1.00 0.97 0.93 0.97 0.002 0.003 0.003 0.002 0.004 0.005 0.004 0.005
0.003 0.003 0.002 0.004 0.97 1.00 0.98 0.98 0.002 0.002 0.001 0.002 0.003 0.006 0.003 0.004
0.004 0.005 0.004 0.004 0.93 0.98 1.00 0.98 0.003 0.003 0.002 0.003 0.004 0.004 0.005 0.005
0.004 0.003 0.003 0.002 0.97 0.98 0.98 1.00 0.003 0.005 0.003 0.003 0.003 0.004 0.003 0.006
cactus 0.001 0.001 0.001 0.001 0.002 0.002 0.003 0.003 1.00 0.98 0.96 0.98 0.002 0.003 0.004 0.002
0.002 0.002 0.002 0.001 0.003 0.002 0.003 0.005 0.98 1.00 0.93 0.98 0.003 0.003 0.003 0.003
0.001 0.001 0.001 0.001 0.003 0.001 0.002 0.003 0.96 0.93 1.00 0.81 0.003 0.003 0.004 0.003
0.002 0.002 0.002 0.001 0.002 0.002 0.003 0.003 0.98 0.98 0.81 1.00 0.010 0.007 0.010 0.007
cake 0.005 0.005 0.005 0.004 0.004 0.003 0.004 0.003 0.002 0.003 0.003 0.010 1.00 0.97 0.96 0.97
0.006 0.006 0.008 0.006 0.005 0.006 0.004 0.004 0.003 0.003 0.003 0.007 0.97 1.00 0.96 0.98
0.006 0.007 0.007 0.005 0.004 0.003 0.005 0.003 0.004 0.003 0.004 0.010 0.96 0.96 1.00 0.97
0.006 0.005 0.008 0.004 0.005 0.004 0.005 0.006 0.002 0.003 0.003 0.007 0.97 0.98 0.97 1.00

Intra-class relations and Class-aware alignment (during training)	Intra-class relations on target domain only (during testing)
painting→real	

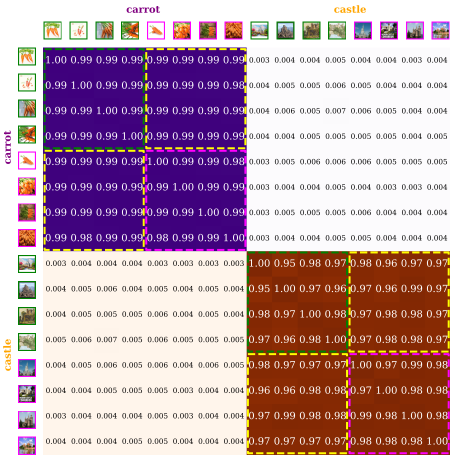

	carrot								castle							
carrot	1.00	0.99	0.99	0.99	0.99	0.99	0.99	0.99	0.003	0.004	0.004	0.005	0.004	0.004	0.003	0.004
	0.99	1.00	0.99	0.99	0.99	0.99	0.99	0.98	0.004	0.005	0.005	0.006	0.005	0.004	0.004	0.004
	0.99	0.99	1.00	0.99	0.99	0.99	0.99	0.99	0.004	0.006	0.005	0.007	0.006	0.005	0.004	0.004
	0.99	0.99	0.99	1.00	0.99	0.99	0.99	0.99	0.004	0.004	0.005	0.005	0.005	0.005	0.004	0.005
	0.99	0.99	0.99	0.99	1.00	0.99	0.99	0.98	0.003	0.005	0.006	0.006	0.006	0.005	0.005	0.005
	0.99	0.99	0.99	0.99	0.99	1.00	0.99	0.99	0.003	0.004	0.004	0.005	0.004	0.003	0.003	0.004
	0.99	0.99	0.99	0.99	0.99	0.99	1.00	0.99	0.003	0.005	0.005	0.005	0.006	0.004	0.004	0.004
	0.99	0.98	0.99	0.99	0.98	0.99	0.99	1.00	0.003	0.004	0.004	0.005	0.005	0.004	0.004	0.004
castle	0.003	0.004	0.004	0.004	0.003	0.003	0.003	0.003	1.00	0.95	0.98	0.97	0.98	0.96	0.97	0.97
	0.004	0.005	0.006	0.004	0.005	0.004	0.005	0.004	0.95	1.00	0.97	0.96	0.97	0.96	0.99	0.97
	0.004	0.005	0.005	0.005	0.006	0.004	0.005	0.004	0.98	0.97	1.00	0.98	0.97	0.98	0.98	0.97
	0.005	0.006	0.007	0.005	0.006	0.005	0.005	0.005	0.97	0.96	0.98	1.00	0.97	0.98	0.98	0.97
	0.004	0.005	0.006	0.005	0.006	0.004	0.006	0.005	0.98	0.97	0.97	0.97	1.00	0.97	0.99	0.98
	0.004	0.004	0.005	0.005	0.005	0.003	0.004	0.004	0.96	0.96	0.98	0.98	0.97	1.00	0.98	0.98
	0.003	0.004	0.004	0.004	0.005	0.003	0.004	0.004	0.97	0.99	0.98	0.98	0.99	0.98	1.00	0.98
	0.004	0.004	0.004	0.005	0.005	0.004	0.004	0.004	0.97	0.97	0.97	0.97	0.98	0.98	0.98	1.00

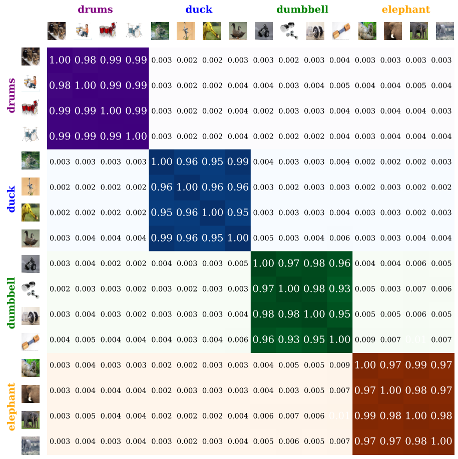

	drums				duck				dumbbell				elephant			
drums	1.00	0.98	0.99	0.99	0.003	0.002	0.002	0.003	0.003	0.002	0.003	0.004	0.003	0.003	0.003	0.003
	0.98	1.00	0.99	0.99	0.003	0.002	0.002	0.004	0.004	0.003	0.004	0.005	0.004	0.004	0.005	0.004
	0.99	0.99	1.00	0.99	0.003	0.002	0.002	0.004	0.002	0.003	0.003	0.004	0.003	0.004	0.004	0.003
	0.99	0.99	0.99	1.00	0.003	0.002	0.002	0.004	0.002	0.002	0.002	0.004	0.003	0.004	0.004	0.004
duck	0.003	0.003	0.003	0.003	1.00	0.96	0.95	0.99	0.004	0.003	0.003	0.004	0.002	0.002	0.002	0.003
	0.002	0.002	0.002	0.002	0.96	1.00	0.96	0.96	0.003	0.002	0.003	0.003	0.002	0.003	0.002	0.002
	0.002	0.002	0.002	0.002	0.95	0.96	1.00	0.95	0.003	0.003	0.003	0.004	0.003	0.003	0.002	0.003
	0.003	0.004	0.004	0.004	0.99	0.96	0.95	1.00	0.005	0.003	0.004	0.006	0.003	0.003	0.004	0.004
dumbbell	0.003	0.004	0.002	0.002	0.004	0.003	0.003	0.005	1.00	0.97	0.98	0.96	0.004	0.004	0.006	0.005
	0.002	0.003	0.003	0.002	0.003	0.002	0.003	0.003	0.97	1.00	0.98	0.93	0.005	0.003	0.007	0.006
	0.003	0.004	0.003	0.002	0.003	0.003	0.003	0.004	0.98	0.98	1.00	0.95	0.005	0.005	0.006	0.005
	0.004	0.005	0.004	0.004	0.004	0.003	0.004	0.006	0.96	0.93	0.95	1.00	0.009	0.007	0.01	0.007
elephant	0.003	0.004	0.003	0.003	0.002	0.002	0.003	0.003	0.004	0.005	0.005	0.009	1.00	0.97	0.99	0.97
	0.003	0.004	0.004	0.004	0.002	0.003	0.003	0.003	0.004	0.003	0.005	0.007	0.97	1.00	0.98	0.97
	0.003	0.005	0.004	0.004	0.002	0.002	0.002	0.004	0.006	0.007	0.006	0.01	0.99	0.98	1.00	0.98
	0.003	0.004	0.003	0.004	0.003	0.002	0.003	0.004	0.005	0.006	0.005	0.007	0.97	0.97	0.98	1.00

Table 17: The similarity matrix $\tilde{S}$ of the 7 SSDA tasks on the **DomainNet** dataset.

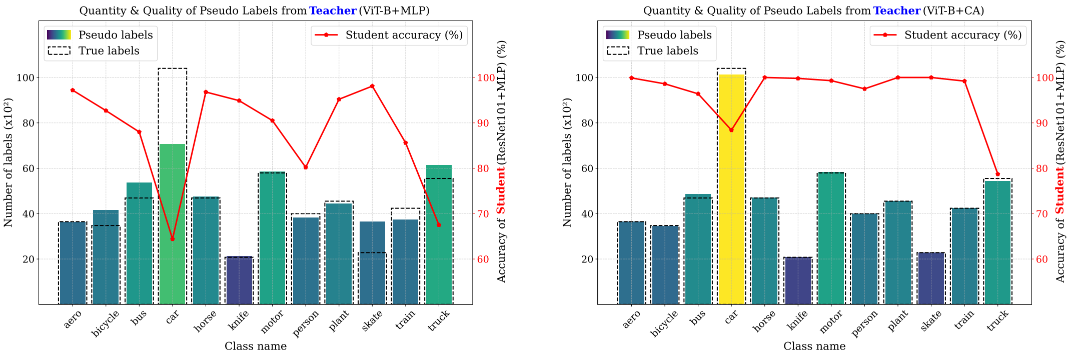

(a) ViT-B+MLP (**Setting 1**)

(b) ViT-B+CA (**Setting 2**)

Figure 7: Comparison of the quantity and quality of pseudo labels between two different teachers (a) ViT-B+MLP and (b) ViT-B+CA on **VisDA2017** under the UDA setting. The bar plots illustrate the number of true labels (outlined in dash lines) and pseudo labels (filled with color) across 12 classes. The red line represents the classification accuracy of the student network (ResNet101+MLP) for each class.

Art→Clipart		
ResNet50	ResNet34	ResNet18
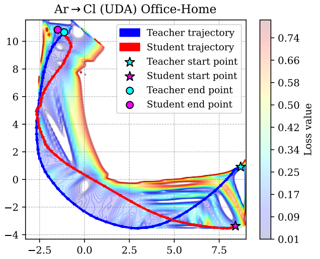	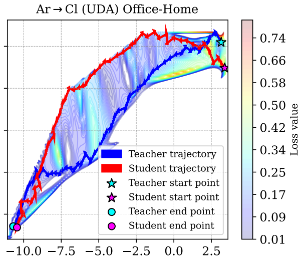	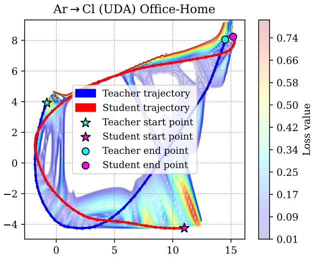
Art→Product		
ResNet50	ResNet34	ResNet18
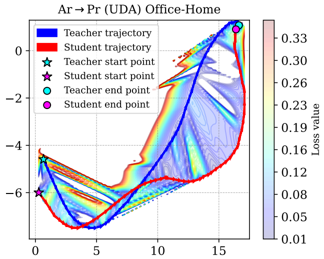	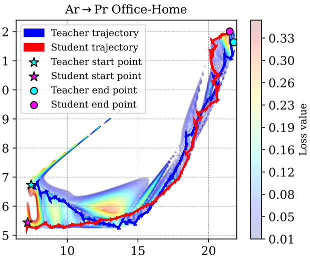	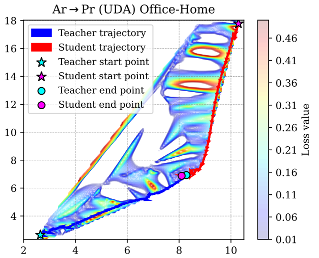
Product→Art		
ResNet50	ResNet34	ResNet18
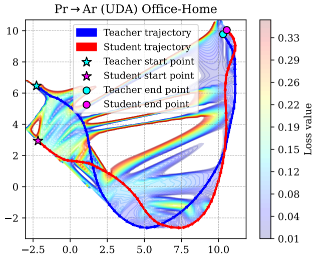	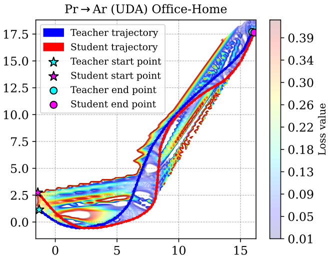	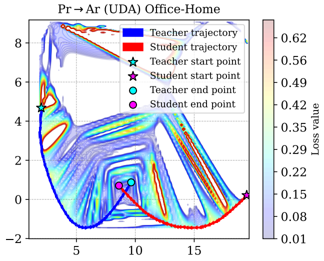
Real→Clipart		
ResNet50	ResNet34	ResNet18
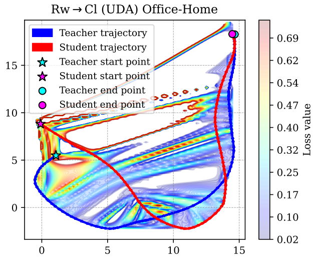	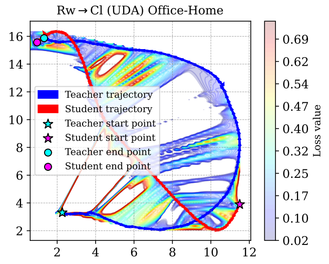	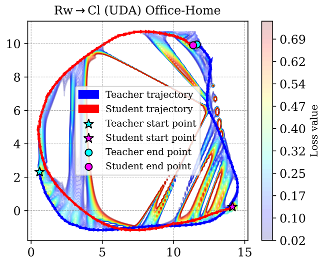

Table 18: 2D visualization of the convergence trajectory in the loss landscape of the teacher network with various student networks.

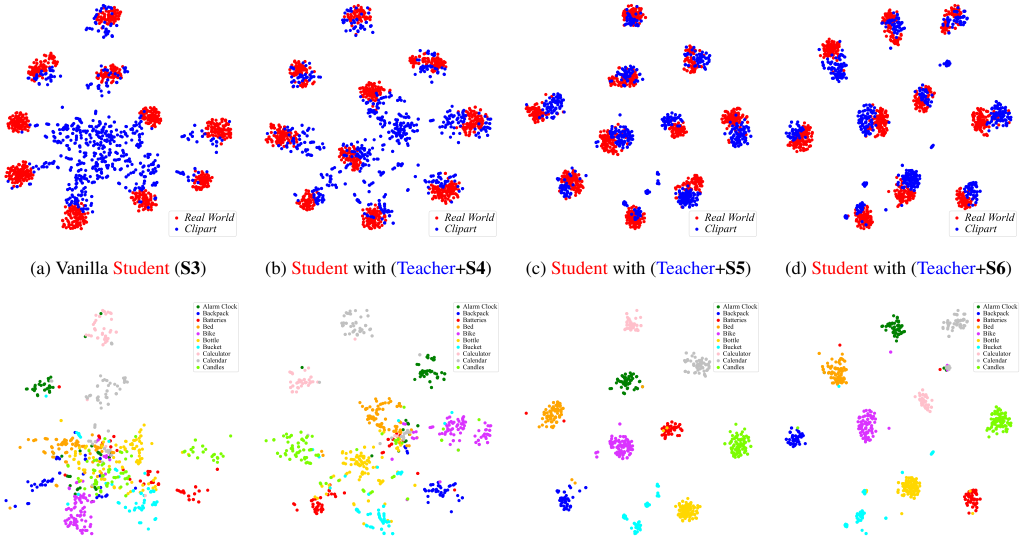

(a) Vanilla Student (**S3**) (b) Student with (Teacher+**S4**) (c) Student with (Teacher+**S5**) (d) Student with (Teacher+**S6**)

(e) Vanilla Student (**S3**) (f) Student with (Teacher+**S4**) (g) Student with (Teacher+**S5**) (h) Student with (Teacher+**S6**)

Figure 8: Feature visualization of the student network under different settings. We use t-SNE to visualize for 10 classes of the *Real World→Clipart* task on **Office-Home** under the UDA setting. In (a) and (e), the student network is trained by setting **S3** without the support of teacher guidance. In (b), (c), (d), (f), (g), and (h), the student network is guided by the teacher network, progressively adding **S4** (Supervised), **S5** (Self-Enhanced), and **S6** $\left(\mathcal{L}_{cc}^{T}(p_T(x_i^{tar}))\right)$, respectively. For easy identification of domain alignment features, source features are represented by red markers, and target features by blue markers in Figs. (a), (b), (c), and (d). Target features are shown in Figs. (e), (f), (g), and (h), we use 10 distinct colors to indicate the 10 classes.

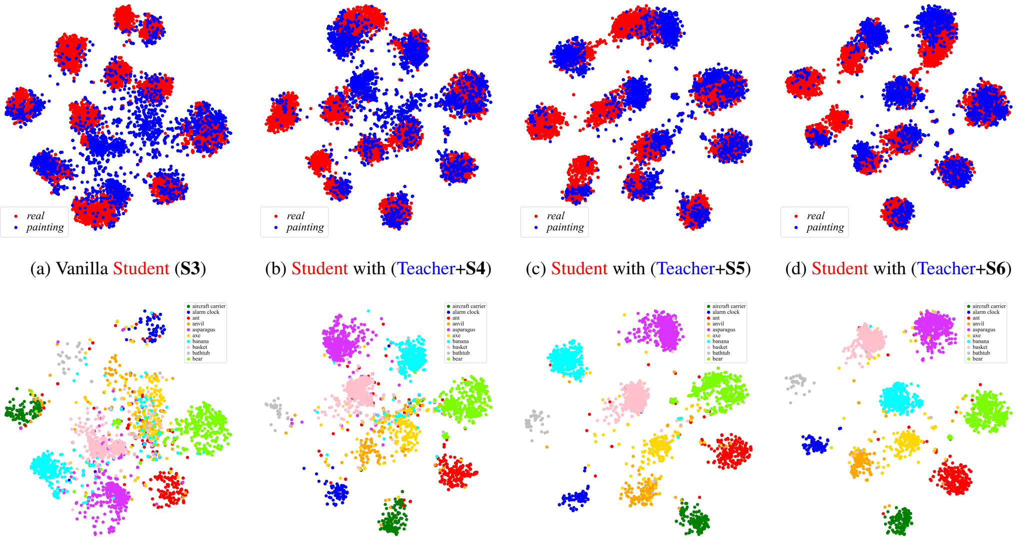

(a) Vanilla Student (**S3**) (b) Student with (Teacher+**S4**) (c) Student with (Teacher+**S5**) (d) Student with (Teacher+**S6**)

(e) Vanilla Student (**S3**) (f) Student with (Teacher+**S4**) (g) Student with (Teacher+**S5**) (h) Student with (Teacher+**S6**)

Figure 9: Feature visualization of the student network under different settings on **DomainNet** (3-shot SSDA, *real→painting*).

Image	Vanilla Student	GraDA (T)	GraDA (S)	**Image**	Vanilla Student	GraDA (T)	GraDA (S)
Art→Clipart							
Alarm clock				Batteries			
	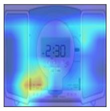	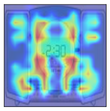			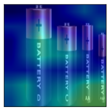	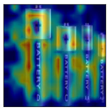	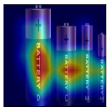
Bed				Keyboard			
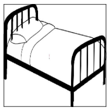	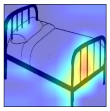	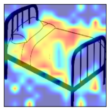	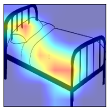	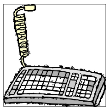	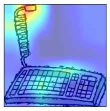	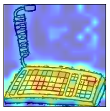	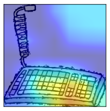
Clipart→Product							
Bottle				Postit notes			
	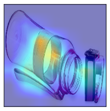	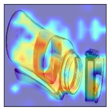	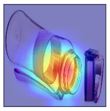	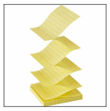	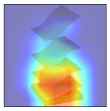	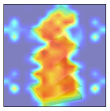	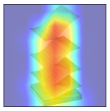
Spoon				Toothbrush			
	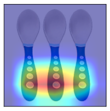	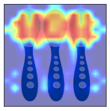	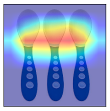		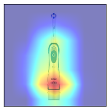	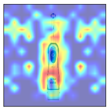	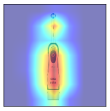
Product→Real World							
Bucket				Chair			
		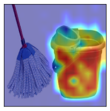	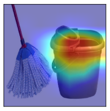		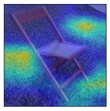	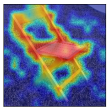	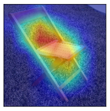
Couch				Toys			
		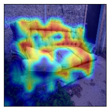			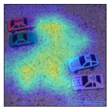	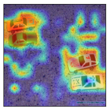	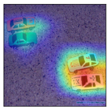
Real World→Art							
Flipflops				Flowers			
	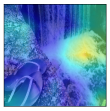	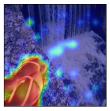	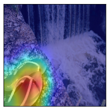		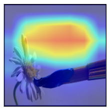	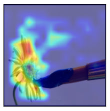	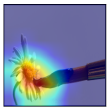
Glasses				Shelf			
	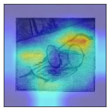	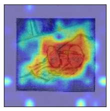	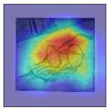	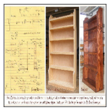	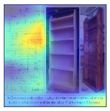	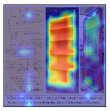	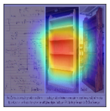

Table 19: Attention maps of the teacher network GraDA (T), and the student network with the vanilla and GraDA (S) variants, on **Office-Home** under the UDA setting. We use Grad-CAM Selvaraju et al. (2017) to identify class-discriminative regions in 4 various samples for each task: Ar→Cl, Cl→Pr, Pr→Rw, and Rw→Ar.

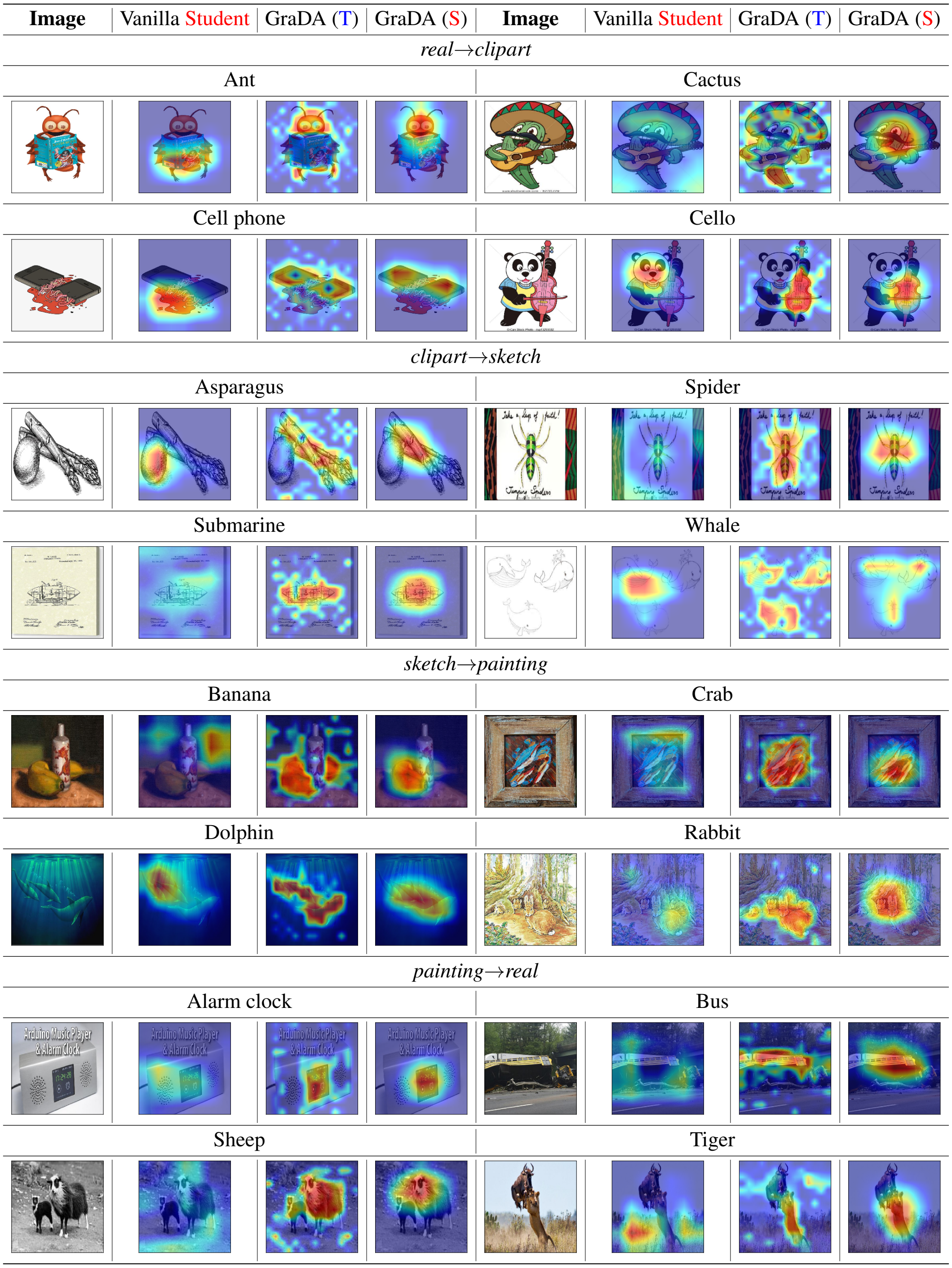

Table 20: Attention maps of the teacher and student networks on **DomainNet** in the 3-shot SSDA setting. The visualization displays class-discriminative regions in 4 diverse samples from the rel→clp, clp→skt, skt→pnt, and pnt→rel tasks.